THE SPECTROSCOPY AND THE PHOTOPHYSICS OF 1,2-BENZAZULENE, A DERIVATIVE OF AZULENE.

A Thesis Submitted to the College of
Graduate and Postdoctoral Studies

In Fulfillment of the Requirements
For the Degree of Master of Science

In the Department of Chemistry,
University of Saskatchewan
Saskatoon

By STEPHEN AWUKU

Permission to Use

In presenting this thesis in partial fulfilment of the requirements for a postgraduate degree from the University of Saskatchewan, I agree that the Libraries of the University make it freely available for inspection. I further agree that permission for copying of this thesis in any manner, in whole or in part, for scholarly purposes may be granted by professor Ronald P. Steer and Amy Stevens, who supervised my thesis work, or in their absence, by the Head of the Department or the Dean of College in which my thesis work was done. It is understood that any copying, publication, or use of this thesis or parts thereof for financial gain shall not be allowed without my written permission. It is also understood that due recognition shall be given to me and the University of Saskatchewan in any scholarly use, which may be made of any material in my thesis.

Requests for permission to copy or to make other use of the material in this thesis in whole or in part should be addressed to:

Head of the Department of Chemistry
University of Saskatchewan
110 Science Place Saskatoon, Saskatchewan (S7N 5C9)

Dean of College of Graduate and Postdoctoral Studies
University of Saskatchewan
116 Thorvaldson Building, 110 Science Place
Saskatoon, Saskatchewan (S7N 5C9)
Canada

Abstract:

The photophysics and the spectroscopy of 1,2-benzazulene were studied both in the liquid and solid phase using azulene for comparison, with the interest of investigating its quenching mechanism from the S_2 state and the possibility of it undergoing singlet fission via $S_2 + S_0 \rightarrow 2T_1$. To understand the quenching mechanism, it is important to, first of all, investigate the similarities and differences in the spectroscopic properties of 1,2-benzazulene and azulene. Steady-state absorption measurement reveals that the S_1-S_0 absorption bands for azulene and 1,2-benzazulene look similar in shape and intensity but very weak compared to their respective S_2-S_0 absorption spectrum. However, the first absorption bands for 1,2-benzazulene are red-shifted compared to azulene. Steady-state fluorescence measurement of these two compounds shows that azulene and 1,2-benzazulene emit anomalous fluorescence emission from the S_2 state. However, unlike azulene, the S_0-S_2 absorption and fluorescence spectra of 1,2-benzazulene reveal an obvious mirror image relationship implying the same transitions are most favourable for absorption and emission at the S_2 state. In addition, there is neither evidence of S_2–S_1 nor S_1–S_0 fluorescence emissions observed for both azulene and 1,2-benzazulene, suggesting that similar to azulene, 1,2-benzazulene also undergo rapid internal conversion from S_1 to S_0 bypassing T_1. Also, 1,2-benzazulene and azulene have been subjected to aggregation studies for comparison. This study is to explore the differences and similarities in their spectroscopy and photophysics at higher concentrations. The results obtained from these experiments reveal that at higher concentrations, there is no clear evidence of fluorescence self-quenching from the S_2 state of 1,2-benzazulene compared to azulene, where fluorescence self-quenching from the S_2 is evident at a similar concentration range. The S_2 fluorescence self-quenching in azulene occurs via a diffusion-controlled process with a static quenching component observed from the Stern-Volmer plots.

The time-dependent diffusion coefficient (K_q) was obtained to be 1.5 x 10^{10} $M^{-1}s^{-1,}$ similar to that obtained by *Reis e Sousa, et al.*[1]. Picosecond transient absorption measurement conducted on the solution phase samples of 1,2-benzazulene gives S_2 lifetime similar to that obtained by non-linear fluorescence upconversion technique. The calculated non-radiative decay rate constant from the S_2 (k_{nrS2}) of 1,2-benzazulene at its measured $\Delta E(S_2 - S_1)$ reveals an energy gap correlation following the same trend as azulene and its fluorinated derivatives. This occurrence suggests that, like azulene and its fluoroderivatives, S_2-S_1 internal conversion is the main decay path for 1,2-benzazulene. Also, the electronic spectra of 1,2-benzazulene show that singlet fission process via $S_2 + S_0 \rightarrow 2T_1$ would be near thermoneutral. However, the electronic spectra obtained for the 1,2-benzazulene solid thin film reveal the formation of aggregates with no measurable S_2 fluorescence, suggesting ultra-fast processes happening likely, singlet fission. The mechanism for this ultrafast process in 1,2-benzazulene thin film is yet to be explored.

Acknowledgement

First, I would like to thank my supervisors, Ron Steer, Ph.D. and Amy Stevens, Ph.D., for their continuous advice, support, guidance, and patience over the past two years. I am incredibly grateful to them for their immense contributions to my research work.

I would also like to thank my academic committee, Tara Kahan, Ph.D., for her expert advice, George Belev Ph.D. for his selfless help in training me to use the TSCPC instrument and our Collaborators from the University of Melbourne, Australia, for their efforts geared towards the success of my research work, including Siobhan J. Bradley, Kenneth P. Ghiggino, Jonathan M. White and Colleen Yeow.

Many thanks also go to the members of my research group Darshi and Ozra, including all the graduate students in Paige's group and other research groups who have both directly and indirectly helped in my research work with valuable information and guidance; Alfred, Srikant, David, Jeveria and Chase (Tim Kelly's group)

I would also like to thank NSERC and the Department of Chemistry at the University of Saskatchewan for their financial support.

Lastly, many thanks go to my friends and family, especially Shelter Awuku, my father, Patience Tetteh Kwame, my Aunty, for their encouragement and support. I truly appreciate it and hope to make them proud.

Table of Content

List of Figures

List of Tables

List of Abbreviations

A…….	Absorbance
Az……...	Azulene
ADC……...	Analogue-to-digital converter
BBO……...	Beta barium borate
Bz-Az…….	Benzazulene
CW……..	Continuous wave
CFTD…….	Constant fraction timing discriminator
D…….	Delay line
Ds……...	Datastore
1,3-DiF-Az…….	1,3-difluoroazulene
FWHM……...	Full width at half maximum
1-F-Az……	1-fluoroazulene
FRET……..	Förster resonance energy transfer
FTIR……...	Fourier transform infrared
FC……...	Franck-Condon
GSB……	Ground state bleach
HOMO……...	Highest occupied molecular orbital
IRF…….	Instrument response function
IR……...	Infrared
IC……...	Internal conversion
ISC…….	Intersystem crossing
LED……	Leading edge timing discriminator
MCA……..	Multichannel analyzer
MCH……..	Methylcyclohexane

MeOH……	Methanol
MHz……..	Megahertz
N……	Number of atoms
ND…….	Neutral density filters
OPM……..	Off-axis parabolic Mirror
PMT……...	Photomultiplier tube
PMMA……...	Polymethylmethacrylate
QPD……...	Photochemical decomposition quantum yield
SF……...	Singlet Fission
SE……	Stimulated emission
SI…….	Supplementary information
TAC……...	Time-to-amplitude converter
TCSPC……...	Time correlated single photon counting
TAS……	Transient absorption spectroscopy
TTA……	Triplet-triplet annihilation
THF……	Tetrahydrofuran
Tol……..	Toluene
UC……..	Non-linear fluorescence upconversion
UV……..	Ultraviolet
VR……..	Vibrational relaxation
ZnTPP……	Zinc tetraphenylporphyrin

List of symbols and mathematical terms

E……..	Energy
ε……	Molar absorption coefficient
$\bar{\nu}$……	Wavenumber
λ……	Wavelength
μ…….....	micro
Σ…….....	Sum of
τ…….....	Lifetime
C……..	Speed of light
h……	Planck's constant
A…….....	Amplitude
Δ……..	change
≈……	Approximately
ϕ_f…….....	Fluorescence quantum yield
I_0……..	Initial intensity
I_t……	Intensity at time t
a_1……..	Contribution of τ_1 to the overall decay
a_2……..	Contribution of τ_2 to the overall decay
Γ……	Radiative decay rate constant
Σk_{nr}……...	Sum of radiationless decay rate constant
τ_1, τ_2……..	Average excited state lifetimes
τ_n……..	Natural or intrinsic lifetime
f…….	Oscillator strength
α_1, α_2…….	Amplitudes of the biexponential components of the fluorescence decay

τ_0, τ…… Fluorescence lifetime in the absence and presence of a quencher

F_0, F……... Fluorescence intensity in the absence and presence of a quencher

k_Q…….. Stern-Volmer quenching rate constant

k_q……... Bimolecular quenching rate constant,

[Q]…… Concentration of quencher

Chapter 1: Introduction

The subject of this thesis is the spectroscopy and photophysics of azulene and one of its derivatives, benzazulene. The high level of interest in these polyaromatic compounds is due to the so-called anomalous fluorescence from azulene's second excited singlet state, S_2, as first reported in 1955 by *Beer and Longuet-Higgins*[2]. The findings by Beer and Longuet-Higgins have paved the way for further investigations to be done on azulene and its derivatives; typical among them is the ability of azulene to undergo self-quenching of S_2 as proposed by *Reis, et al.*[1]. The research work by *Reiss and coworkers* have raised so many concerns as to what process could have led to the self-quenching of azulene. Perhaps, singlet fission is a probable guess, as suggested by *Nickel, et al.*[3]. However, other nonradiative processes could have also led to this phenomenon (quenching). It is known that derivatives of azulene compounds could have more enhanced properties than the azulene itself; an example is benzazulene. To date, little is known or documented on the spectroscopy and the photophysics of benzazulene both in solutions and solid thin films. This thesis studied benzazulene in solutions and solid thin films using fluorescence and spectroscopic techniques to understand its electronic and photophysical properties. The techniques used and the theory needed to understand the results obtained from this research work are discussed in the subsequent paragraphs.

1.1 An introduction to photophysics

The natural and artificial types of photo-processes resulting from photon absorption have broad and numerous applications, including photosynthesis, bioluminescence, photodynamic therapy, ozone formation and depletion, and vision. These processes occur when a molecule becomes energetically excited after the absorption of photons. In dissipating the absorbed energy from the excited state, one of these two phenomena is likely to happen, a chemical change in the molecule (photochemistry) or a physical change in the molecule (photophysics). In this thesis, photophysical processes are the major phenomenon witnessed in this research work, mainly radiationless (internal conversion, intersystem crossing and vibrational relaxation) and radiative processes (fluorescence and phosphorescence). Figure 1.1 shows a simplified Jablonski diagram used to explain the electronic transitions discussed below.

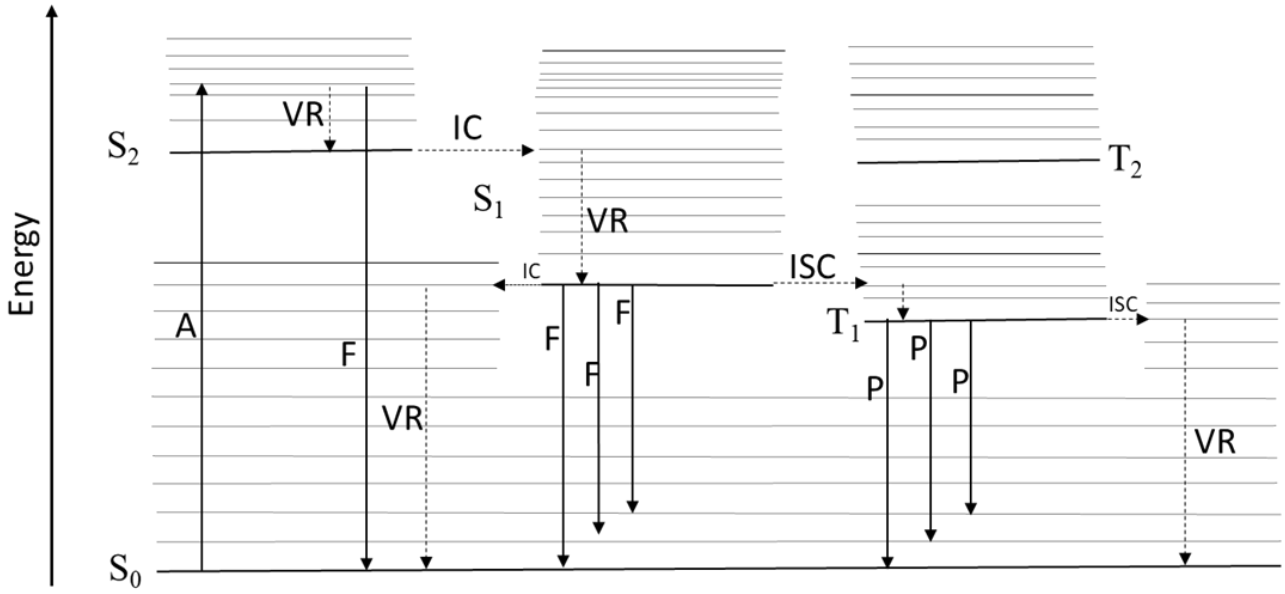

Figure 1.1: A simplified Jablonski diagram. A = absorbance, F = fluorescence, P = phosphorescence, ISC = intersystem crossing, IC = internal conversion, VR = vibrational relaxation, S_0 = ground singlet state, S_1 = first excited singlet state, S_2 = second excited, T_1 = first excited triplet state, T_2 = Second excited triplet state. The figure represents the electronic arrangement of the excited state and the radiative and non-radiative pathways.

Fluorescence is the radiative decay of a molecule from its excited singlet state to the ground singlet state, with a wavelength dictated by the energy gap spacing between the excited and ground singlet states. Also, the spin multiplicity between the electronic states is the same in a radiative decay process (from $S_2 \rightarrow S_0$, for example). There are other excited states like S_3 and S_4; however, fluorescence emissions are usually studied from the $S_1 \rightarrow S_0$ depending on the type of molecule under study. As described above, the S_0 represents the singlet ground state, S_1, S_2, S_3 and S_4 denotes the first, second, third and fourth singlet excited state, respectively. At room temperature, molecules are initially allowed to populate the singlet ground state which has all of its electron spins paired and occupies the orbital of the lowest energy level (Aufbau and Pauli's Principle).

From the higher excited state, the molecules may return to the ground state via a radiationless process. An example is internal conversion (IC), in which a possibility exists that the excited molecule can move from a vibrational energy level in one electronic state, say S_2, to another vibrational energy level in a lower electronic state, say S_1[4]. It could also happen that the excited state energy could be dissipated by another non-radiative pathway known as intersystem crossing (ISC). In ISC, the relaxation pathway occurs between excited states of different spin multiplicity, say an electronic transition from $S_1 \rightarrow T_1$ where T_1 represents the first excited triplet state in which the two unpaired electrons in this state are of parallel spins different from that of S_1[5]. Intersystem crossing (ISC) is a less likely process than internal conversion since the spin multiplicity is not conserved as such, it happens more slowly than internal conversion[5,6]. After ISC, there could be an electronic transition from $T_1 \rightarrow S_0$ accompanied by photon emission. In this case, the luminescence detected is called phosphorescence. Though it was established that $T_1 \rightarrow S_0$ electronic transition is forbidden based on the spin-multiplicity selection rule[7], this radiative process (phosphorescence) rather happens at a slow rate due to the significant interaction between

spin and orbital angular momentum (spin-orbit coupling). In this thesis, much emphasis would be placed on fluorescence whereas phosphorescence would not be discussed further. It is worthy to note that at the triplet state, there could also be triplet-triplet annihilation (TTA) which will later be considered in this chapter.

From figures 1.1 and 1.3, in between each electronic state are vibrational states where molecules usually populate at thermal equilibrium based on Boltzmann's distribution. At room temperature, most molecules occupy the lowest vibrational energy level of the electronic ground state. However, very few molecules have sufficient internal energy at ambient temperatures to occupy a higher vibrational state of the ground electronic state before any transition to a higher electronic state. Also, in between vibrational states are rotational states. In general, normal modes are used to describe the vibration of polyatomic molecules. Each normal mode is characterized by simultaneous vibration of different parts of the molecule. A nonlinear molecule exhibits 3N-6 vibrational normal modes for N number of atoms. In contrast, a molecule with a linear molecular structure has 3N-5 normal vibration modes. In this thesis, the molecule of interest is a nonlinear polyatomic molecule.

Molecules practically always go through vibrational relaxation (loss of energy in the absence of light emission) during their excited state lifetime. Also, the molecule's environment plays a vital role in the molecule's vibrational relaxation process. In condensed phases, the excess vibrational energy produced is converted to heat and subsequently absorbed by solvent molecules upon collision with the excited state fluorophores[8] (intermolecular vibrational relaxation). In the case where there is negligible interaction between the molecule of interest and its environment, all the vibrational energy is shared among all the vibrational modes of the molecule (intramolecular vibrational relaxation) which can take place in condensed phases and gases but very fast in solids[9]. Vibrational relaxation in condensed media is exceptionally a fast process (picosecond or less) as

such, most S_1 (Kasha's rule) and S_2 (Anti-Kasha's rule) fluorescence emission usually starts from the lowest vibrational level in the S_1 and S_2 state to a higher vibrational level in the ground electronic state. The same event is noticed for phosphorescence from T_1. Due to these energy losses, fluorescence and phosphorescence emission spectra are red-shifted (longer wavelength) than the absorption spectrum. This phenomenon is generally known as Stokes shift, described by the difference in energy between the maximum peaks in the absorption and emission spectra (figure 1.2). Stokes shift can be observed in most fluorophores used in solution investigations[10]

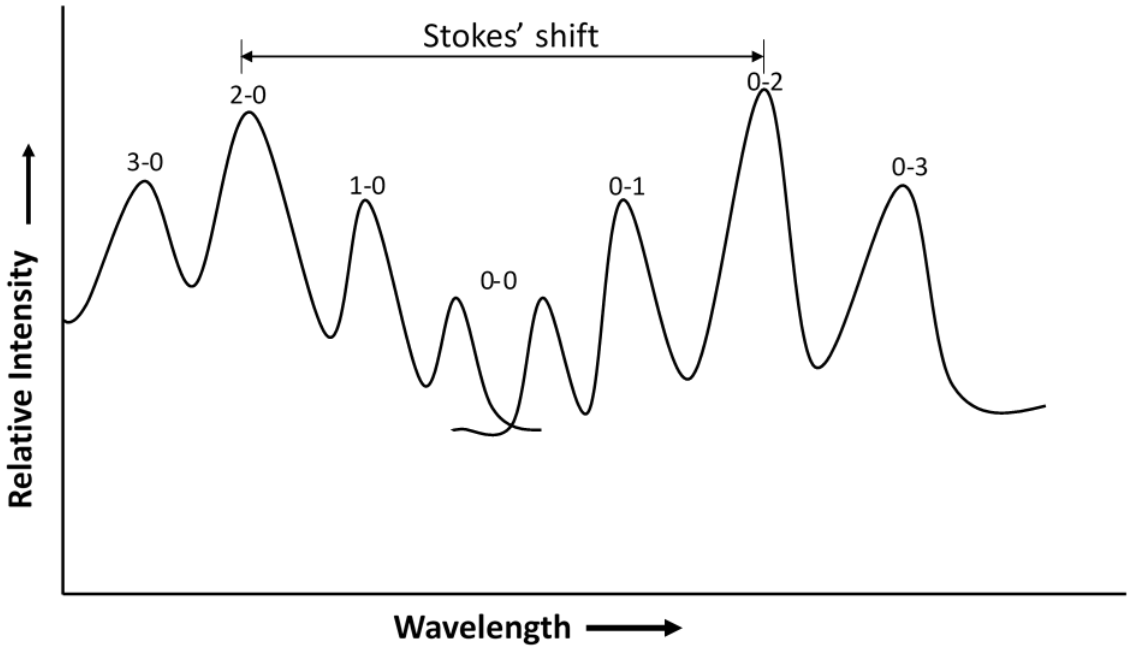

Figure 1.2: A schematic diagram showing the mirror image rule and Stokes shift.

In the case where there are same transitions and similarities between vibrational energy levels in both absorption and emission processes, the spectra obtained from these processes can be symmetrical (mirror image) to each other as predicted by Franck-Condon. That is, if a particular transition probability (Franck-Condon factor) between the zeroth and second vibrational levels is largest in absorption, then a similar transition is likely to occur in emission provided that there is

no large geometry difference between the two electronic states. According to the Franck-Condon principle, radiative electronic transitions between states occur with no significant change in the position of the nuclei.[11].

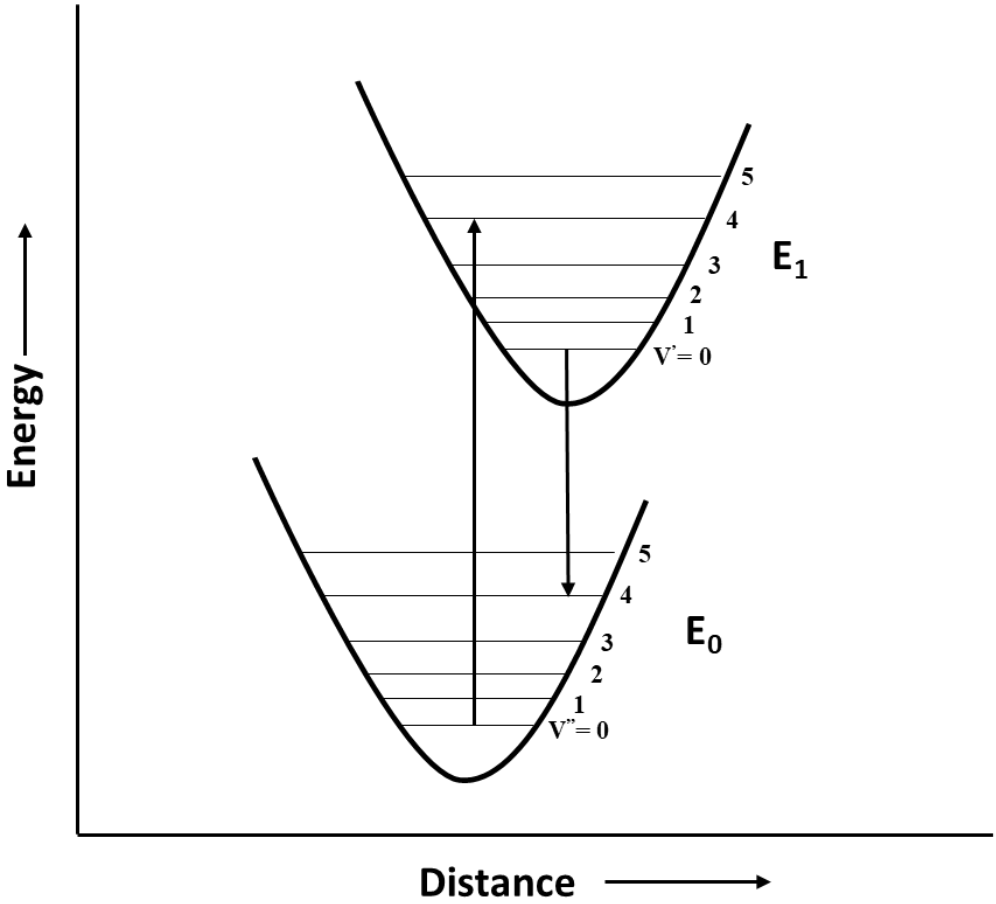

Figure 1.3: An energy diagram of the Franck-Condon Principle. The potential energy surfaces illustrate favorable electronic transitions between v = 0 and v'= 4.

The allowedness of an electronic transition between energy levels of a molecule during absorption or emission process is described using the oscillator strength. The oscillator strength has no unit and is calculated by integrating the area under the curve of the absorption spectrum at selected wavenumber regions. The expression for the oscillator strength is given as

$$f = 4.32x10^{-9}\ \text{mol cm}^2\text{L}^{-1} \int \varepsilon\, d\, \bar{\nu} \qquad \text{eqn (1.1)}$$

where ε is the molar absorption coefficient having the unit L mol^{-1} cm^{-1} and the $\bar{\nu}$ is the wavenumber in cm^{-1}.

The measurable factors that can be used to determine a molecule's fluorescence emission include the wavelength range of photon absorption and emission, the orientation variations between absorption and emission of photons (anisotropy or polarisation), the quantum yield and finally, the emission rate (decay times). The fluorescence quantum yield (Φ_F) is the fraction of electronically excited molecules that return to the ground state with fluorescent emission. It is mathematically expressed as

$$\phi_F = \frac{\Gamma}{\Gamma + \sum k_{nr}} \qquad \text{eqn (1.2)}$$

where Γ and Σk_{nr} are the radiative and the sum of all non-radiative decay rate constants. The quantum yield can be near unity if the radiationless decay rate is relatively much smaller (negligible) than the radiative decay rate constant, that is $k_{nr} << \Gamma$. In other instances where non-radiative pathways compete efficiently with fluorescence emission, the fluorescence quantum yield becomes less than one.

The average duration a molecule spends in the excited state before transitioning to the ground state without electronic quenching is the lifetime of the molecule at the excited state. This can be calculated using the expression:

$$\tau = \frac{1}{\Gamma + k_{nr}} \qquad \text{eqn (1.3)}$$

Also, the lifetime of a molecule undergoing only radiative process is termed as the intrinsic or natural lifetime of that molecule. and mathematically defined as

$$\tau_n = \frac{1}{\Gamma} \qquad \text{eqn (1.4)}$$

where Γ is the radiative decay rate constant. Rearrangement of eqn (1.2), (1.3) and (1.4) can help determine the natural lifetime knowing the measured lifetime and the quantum yield. The mathematical relation is also expressed as

$$\tau_n = \frac{\tau}{\phi_F} \qquad \text{eqn (1.5)}$$

Also, an exponential function is used to describe the decay of fluorescence intensity with time in a uniform population of molecules excited by a short pulse of laser light. Molecules that decay from the excited state following the expression below exhibit first-order kinetic behaviour as expressed in eqn (1.6). I_t represents the intensity at a time "t," and I_0 represents the initial intensity.

$$I_t = I_0 e^{\frac{-t}{\tau}} \qquad \text{eqn (1.6)}$$

Additionally, an excited fluorophore may undergo structural changes and can interact with solvent molecules or other molecules. These occurrences could lead to multi-exponential decay being observed from the sample under study. For instance, bi-exponential decays have two lifetime components[4]. In this case, another parameter is added to eqn (1.6) to form eqn (1.7). The expression below represents the second-order decay function used to ascertain the two lifetime components of the molecule at the excited state.

$$I_t = \alpha_1 e^{\frac{-t}{\tau_1}} + \alpha_2 e^{\frac{-t}{\tau_2}} \qquad \text{eqn (1.7)}$$

where α_1, α_2, τ_1 and τ_2 represent the amplitudes and decay times of the biexponential components of the fluorescence decay. The sum of the amplitudes is always equal to one.

1.2 Azulenes

Azulene, $C_{10}H_8$, is a nonalternant aromatic bicyclic isomer of naphthalene. Figure 1.4 shows the resonance delocalization structure of azulene, where the tropylium ring is electron deficient. In contrast, the five-membered ring is electron-rich, which results in a dipole moment of 0.7 D corresponding to the ground state of azulene, as reported by *Hochstrasser, et al.*[12].

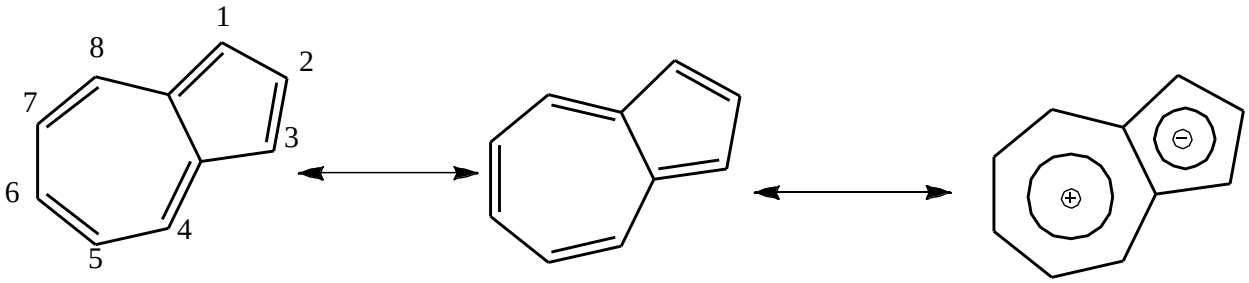

Figure 1.4: The molecular and resonance structure of azulene and how the carbons in the ring are being numbered are shown here. These structures were drawn using ChemDraw software.

Azulene is a 10π electron system and has aromatic properties. Its peripheral bonds have approximately similar lengths. Also, it undergoes Friedel-Crafts-like substitution. The π-molecular orbitals of azulene molecules exhibit an unusual structure and arrangement, as a result of which it undergoes anti-Kasha fluorescence decay from an upper excited state to the ground state ($S_2 \rightarrow S_0$)[13]. The anomalous fluorescence emission in azulene is due to its low-lying S_1 state, which brings to light a large energy gap difference between its S_1 and S_2 states. This large energy gap between the first and second excited singlet state disfavors the intersection of potential energy surfaces and results in small F-C factors for IC, rendering radiationless transitions from the upper to the lower state ($S_2 \rightarrow S_1$) improbable. Hence, the anomalous fluorescence from $S_2 \rightarrow S_0$ becomes a more likely transition to be observed[2,13–15]. The quantum yields for S_2 and S_1 fluorescence of azulene in methanol were estimated to be 0.24 and $2x10^{-6,}$ respectively[16]. Also, the excited state lifetime of

the S_2 and S_1 states for azulene fluorescence fall between the ranges of 1- 2 ns and 0.5 – 5 ps for several solvents, respectively[17].

Azulene, as an example of nonalternant hydrocarbon, has its optical property different from its isomer, naphthalene. As previously mentioned, azulene is blue due to the weak $S_0 \rightarrow S_1$ absorption observed in the visible region resulting from the weak electron density overlap between its HOMO and LUMO, leading to a much narrower space between the S_1 and S_0[18]. Azulene also displays a distinct near UV absorption peak assignable to $S_0 \rightarrow S_2$ electronic transition[19]. On the other hand, the white colour associated with naphthalene is due to the optical transition between S_0-S_1. The S_0-S_1 transition is the major electronic transition observed for naphthalene in the ultra-violet (UV) region hence the white colour[14,19].

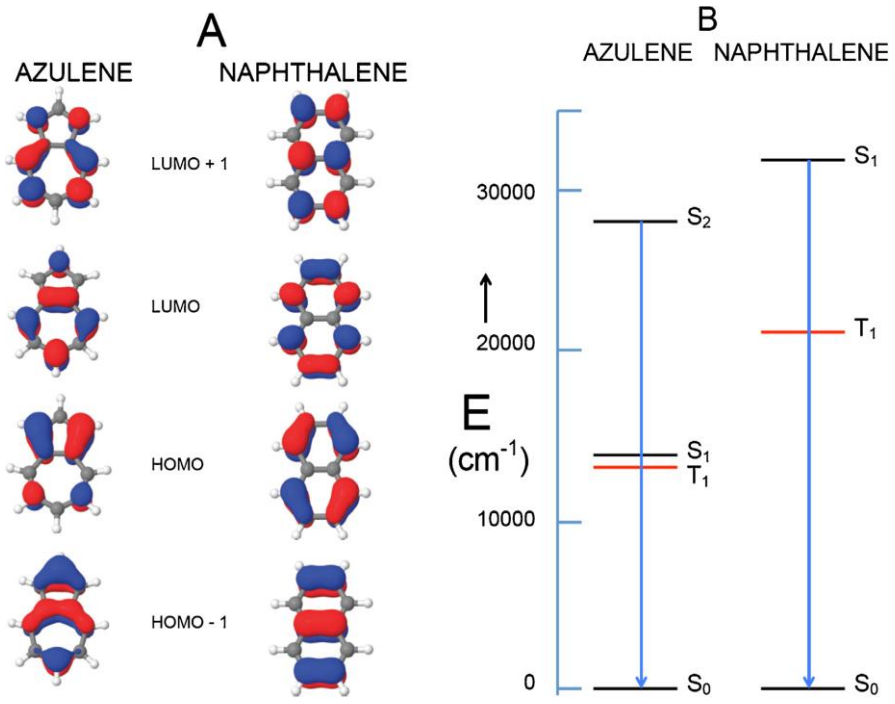

Figure 1.5 A: indicates the frontier molecular orbitals of azulene compared to that of naphthalene. B: shows the comparison of electronic energy spacings of the radiative transitions observed in normal naphthalene and anomalous azulene fluorescence. Figure reproduced from reference.[19]

Figure 1.5 above highlights the electronic transitions observed in azulene compared to naphthalene. The molecular orbitals of naphthalene are mirror related (an identical and symmetrical arrangement of frontier orbitals) see figure 1.5A. As such, the LUMO and the HOMO reside in the same regions of space[20]. In contrast, azulene shows a small energy gap difference between the first excited singlet state (S_1) and the ground state (S_0), which occurs as a result of the geometry of the non-mirror-related HOMO-LUMO (unsymmetrical arrangement of frontier orbitals) that decreases the repulsive interaction between the two unpaired electrons present in these frontier orbitals in S_1[2,14,15,19]. In azulene, the HOMO-1 and LUMO and/or HOMO and LUMO+1 play a significant role in the electronic transition to the S_2 state. The presence of unpaired electrons in these frontier molecular orbitals in S_2, π-π^* state overlap effectively compared to the HOMO and LUMO in the S_1 state. Due to the substantial overlap between the frontier orbitals at the S_2 state, the energy spacing between azulene's S_2 state and its S_0 state is wide but marginally less than that observed in the S_0-S_1 state of naphthalene[12,21] as illustrated in figure 1.5 B. The large energy gap between the ground state (S_0) and the first excited singlet state (S_1) found in naphthalene relative to azulene occurs due to a strong coulombic repulsion between the electron densities of the HOMO and the LUMO resulting from the effective overlap of this frontier orbitals[22]

Liu and coworkers reported that substituting electron-donating or electron-withdrawing groups at odd or even-numbered positions of the azulene ring modifies its electronic properties. These modifications were determined based on the calculation of the electron distributions of the azulene's molecular orbitals[15,19,21].

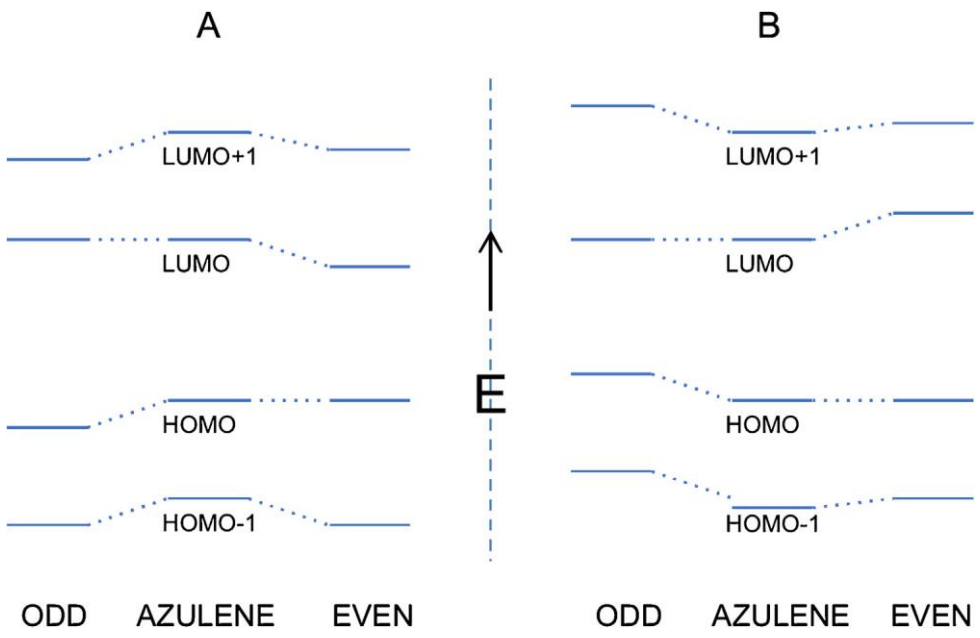

Figure 1.6. The effects of electron-withdrawing and electron-donating groups at even and odd-numbered positions of the azulene ring in the S_1 and S_2 states, which includes the HOMO-1, HOMO, LUMO and LUMO+1. A: shows electron-withdrawing groups substituted at both even and odd-numbered positions, B: substituting electron-donating groups. Figure reproduced from reference.[19].

The researchers suggested a decrease in the HOMO-LUMO gap and an increase in LUMO-LUMO+1 separation by substituting electron-donating groups at an odd-numbered position (1,3,5 and 7) and electron-withdrawing groups at even-numbered (2,4,6 and 8) sites of the azulene ring. Similarly, these researchers reported an increase in the HOMO-LUMO gap and a decrease in the LUMO-LUMO+1 separation when electron-withdrawing substituents are substituted at odd-numbered positions or electron-donating substituents at even-numbered sites of the azulene ring[20] as indicated in figure 1.6.

To explain this phenomenon's details, it is suggested in the literature that the S_0-S_2 transition in azulenes are significantly influenced by the HOMO and LUMO+1, with their nodes at positions 2 and 6 coupled with very similar electron density distributions[15]. However, the LUMO of azulene is different compared to the HOMO and LUMO+1. The LUMO has very low electron density at odd-numbered positions and high electron density at even-numbered locations,

whereas the HOMO and LUMO+1 have high electron density at the odd-numbered sites of the azulene ring. Therefore, substituting electron-donating groups at the odd-numbered positions (1,3,5 and 7) increases the HOMO and LUMO+1 energy level without significantly affecting the energy level of the LUMO, thus increasing $\Delta E(S_2\text{-}S_1)$. Dissimilarly, The LUMO is pushed to a higher energy level, whereas the energy level for the HOMO and LUMO+1 remains almost unchanged level when electron-donating groups are substituted at even-numbered sites (2,4,6 and 8) of the azulene ring. The net effect of this occurrence is a decrease in $\Delta E(S_2\text{-}S_1)$.[15,20], as illustrated in figure 1.6 A. This contrasts with when the substituent is an electron-withdrawing group substituted at even and odd-numbered positions of the azulene ring. The energy level for the HOMO and LUMO+1 remains almost unchanged, but the LUMO decreases in energy level resulting from HOMO-LUMO repulsion. The effect of this occurrence is an increase in the $\Delta E(S_2\text{-}S_1)$. Electron-withdrawing groups substituted at odd-numbered locations reduce the energy level of the HOMO and LUMO+1, but the LUMO remains nearly unchanged, leading to a decrease in $\Delta E(S_2\text{-}S_1)$[23], as shown in figure 1.6.

Jortner, et al.[24]. reported that, in azulene and some of its derivatives and in larger molecules such as zinc tetraphenylporphyrins(ZnTPP), the rate of radiationless decay via $S_2\text{-}S_1$ internal conversion decreases exponentially as the energy gap size between these two states increases and vice versa. This phenomenon is described using the energy gap law. It is mathematically expressed

$$k_{nr} \alpha V^2_{S2-S1} FC \qquad \text{eqn 1.8}$$

where k_{nr} represents the non-radiative decay rate constant, FC is the Franck Condon factor and V^2_{S2-S1} is the electronic interaction between the coupled S_2 and S_1 states. In azulene and its derivatives, there is no significant change in the $V_{S2\text{-}S1}$ however, the Franck Condon factor which

depends on the S_2-S_1 energy gap changes in these groups of molecules and can be mathematically expressed as

$$FC\ \alpha\ (\int \chi_{S2}\chi_{S1})^2 d\tau\ \alpha\ e^{-\gamma\Delta E(S_2-S_1)} \qquad \text{eqn 1.9}$$

where $\chi_{S2}\chi_{S1}$ represents the overlap of the vibrational wavefunction at the S_2 and S_1 state which decreases exponentially as the ΔE (S_2-S_1) increases and vice versa, γ is a term that can be expressed in terms of molecular parameters and C is proportionality constant.

Combining eqn 1.8 and 1.9 yields an overall expression (see eqn 1.10) that describes the exponential change in the non-radiative decay rate constant (k_{nr}) as the S_2-S_1 energy gap varies.

$$In k_{nr} = -\gamma\Delta E(S_2 - S_1) + In V_{S2-S1}^2 + C \qquad eqn\ 1.10$$

From figure 1.5 B, there is a sizeable singlet-triplet splitting in naphthalene. This large splitting is due to the efficient overlap between the unpaired electron density present in the singly-occupied molecular orbitals of the S_1 and S_2 states of naphthalene[25]. In contrast, azulene shows a minimal S_1-T_1 splitting[19,25] because of the weak repulsive interaction between the two unpaired π-electrons present in the HOMO and LUMO in the configuration of azulene. The S_2-T_2 splitting in azulene is large and similar to that found in naphthalene.

As mentioned earlier, much interest has been developed towards azulene and its derivatives, mainly for their unique electronic and photophysical properties. Azulene derivatives have been applied in constructing optoelectronic devices[23], including molecular switches[22], liquid crystals[26], electrochromic materials[18], organic/polymeric conductors[27] and near-infrared resonance materials[28]. In this thesis, the photophysics of benzazulene, a derivative of azulene, will be considered using azulene for comparison.

1.3 Benzazulene

Most benzenoid hydrocarbons, which are alternant in nature, undergo fluorescence emission according to $S_1 \rightarrow S_0$, independent of the orientation of its transition moment[26]. The peripheral bonds of azulene[29] are predicted to have aromatic character and lie between 1.394 and 1.408 Å, as reported by *Gupta, et al.*[29] The fusion of the benzene ring nucleus to azulene does not disrupt the aromatic character of the overall compound but makes the benzazulene conformationally strong, rigid and fixed[27,29].

The structure of benzazulene exists in three isomeric forms depending on the position of the fused benzene ring (a-c). These three isomers are the first of the azulene benzologue series. In this thesis, the focus will be on benz[a]azulene or 1,2-benzazulene. The synthesis of benz[a]azulene was done by our research partners at the University of Melbourne, Australia, as reported in the literature by *Conrow, et al.*[30] and *Sperandio, et al.*[31].

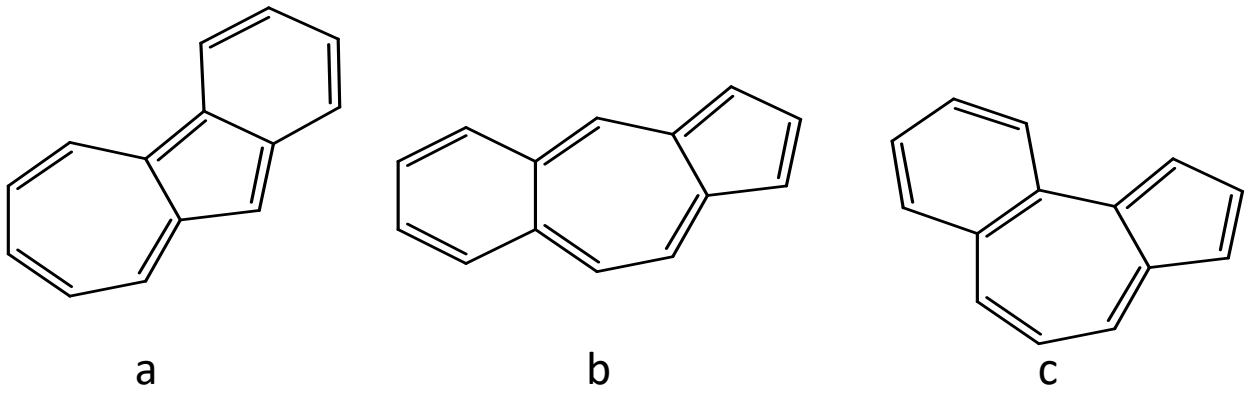

Figure 1.7 The structure of benzazulene[32,33]. a = benz[a]azulene, b = benz[f]azulene, c = benz[e]azulene. These structures were drawn using ChemDraw software.

Considering the electronic behaviour of benzazulene, the π-system of azulene is being enlarged by benzene fusion, which leads to a significantly benzenoid system where the azulene moiety is perturbed as a result of this fusion[34]. In an attempt to explain the electronic structure of benzazulene, *Binsch and coworkers* reported that the perturbation of the azulene ring by the benzene fusion reduces the symmetry of the azulene system from C_{2v} to C_s. These modifications

on the azulene ring are expected to affect the anomalous fluorescence emission from $S_2 \rightarrow S_0$. However, this predicted property change was not seen, and as such, serves as one of the bases for the significant interest in benzazulene[27,32,33,35]

At higher concentrations, azulene and azulene derivatives are known to form multimolecular aggregates[19,36], which are made up of several molecules stacked on top of one another and kept together by π-π interactions. These phenomena can be noticed in solutions and thin polymer films. The orientation of the transition dipole moments on neighbouring molecules determines whether small-molecule chromophores form H-type or J-type aggregates when they assemble in the solid-state or liquid phase. H-aggregates are formed when molecules stack largely face-to-face, whereas J-aggregates are formed when molecules stack primarily based on head-to-tail interaction[37]. The formation of these aggregates has significant ramifications and can either influence a spectrum to be red-shifted, typical for J-type aggregates or blue-shifted for H-type aggregates. The shift in absorption spectrum observed for J and H-type aggregates compared to the monomer is due to exciton splitting. For J-type aggregates, the only probable transition is to the lower exciton state due to the head-to-tail arrangement of molecules. In contrast, for the H-type aggregates, the allowed transition is to the higher exciton state resulting from the face-to-face arrangement of the molecules. In the event where both molecules are aligned obliquely to each other, the higher and lower exciton states are allowed for electronic transition. The consequential effect is band splitting[38]. Also, *Ferguson, et al.* reported that at low temperature (77K) in an organic glassy matrix, stable forms of self-aggregated azulene dimers could be formed[39]. The formation of these aggregated dimers is spectroscopically relevant since they can promote certain events such as fluorescence quenching.

1.4 Fluorescence quenching

Fluorescence quenching describes any process that reduces the fluorescence intensity of a given substance containing fluorophores. Fluorescence quenching occurs as a result of excited state reactions, energy exchange and complex formation between excited state and ground state molecule. Quenching of fluorescence emission can also result from the collisional encounter between an excited state molecule and other molecules present in the solution called the quencher. This type of quenching is referred to as collisional or dynamic quenching. The diffusive encounter between the excited state molecule and the quencher causes the molecule at the excited state to return to the ground state without fluorescence emission. The process of collisional quenching is best described using the well-known Stern-Volmer kinetic equation as illustrated in equations 1.11 and 1.12. Collisional quenching is evident in fairly dilute solutions where the molecules are relatively far apart from each other. In this case, a contact between the excited and ground state molecule is required for this type of quenching process to occur. The process of fluorescence quenching also involves energy transfer from the excited state molecule to the quencher. The extent of this energy transfer depends on the distance between the ground and the excited state molecule. This nonradiative energy transfer can occur via a Dexter or Förster mechanism in highly concentrated samples without necessarily, a contact between the excited state fluorophore and the ground state molecule. For highly concentrated samples, energy transfer between excited state fluorophores and ground state molecules can occur via short-range distances, less than 10 Angstrom (Dexter) or long-range distances, greater than 10 Angstrom to 100 Angstrom (Förster). The effect of this process is fluorescence quenching and is widely known as static quenching.[40].

$$\frac{\tau_0}{\tau} = 1 + k_Q[Q] \qquad \text{eqn (1.11)}$$

The τ_0/τ denotes the ratio of the fluorescence lifetime in the absence and presence of a quencher and k_Q represents the Stern-Volmer quenching rate constant which applies when the quencher

inhibits fluorescence emission by a single reaction and [Q] is the quencher's concentration. Also, it is important to mention that the Stern-Volmer kinetic equation, as illustrated in equation 1.11, is used once the k_Q is considered to be time-independent[1]. However, previous documentation on the kinetics of fluorescence quenching indicates that the quenching rate coefficient is time-dependent for a diffusion-controlled process[41]. Nevertheless, the time dependency of this process is not noticeable on the decay curve analysis but very evident on the Stern-Volmer plot using the ratio of fluorescence quantum yield at several dilute and higher concentrations, as shown in equation 1.9. This work will investigate the mechanism of the fluorescence self-quenching process for azulene using time-resolved, specifically, TCSPC techniques. Due to instrumental limitations, this technique is very suitable to investigate the details of collisional quenching process for fairly dilute solutions. However, at higher concentrations, the non-radiative energy transfer process is very fast due to the proximity of the molecules. In this case, the details of the quenching mechanism which may include static quenching, cannot be fully demonstrated by only the TCSPC technique. Hence, the need to consider the Stern-Volmer plot using the ratio of fluorescence quantum yield (see eqn 1.12), which can be obtained by steady-state fluorescence measurement.

$$\frac{F_0}{F} = 1 + k_q \tau_0 [Q] \qquad \text{eqn (1.12)}$$

The Stern-Volmer kinetic equation (see eqn 1.12) also applies in the case of dynamic quenching. In dynamic quenching, the constant k_Q is the product of the true quenching constant, k_q and the fluorescence lifetime, τ_0 in the absence of a quencher. The k_q is the bimolecular quenching rate constant for the elementary reaction of the excited state with the particular quencher. τ_0 is the unquenched lifetime, and F_0/F represents the fluorescence intensity ratio in the absence and presence of a quencher[42]. One of the contributing factors that may lead to fluorescence quenching is singlet fission.

1.5 Singlet fission (SF)

Singlet fission is a spin-allowed process that involves splitting a singlet exciton into two uncorrelated triplet excitons[43] in a bichromophoric system, as illustrated in figure 1.8. The singlet fission process involves a radiationless transition between two electronic states with the same spin multiplicity.

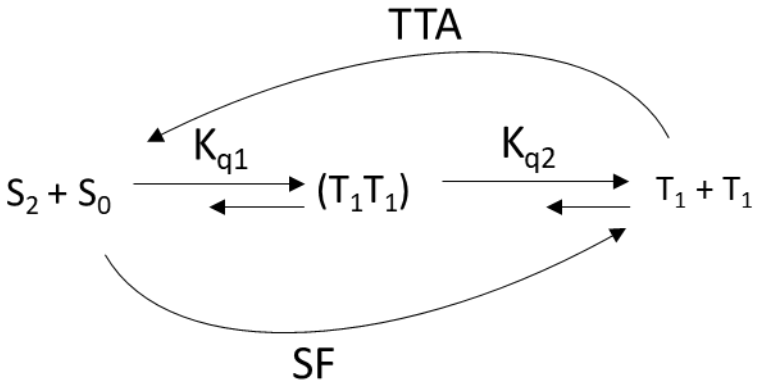

Figure 1.8: A schematic diagram illustrating the kinetic dynamics of singlet fission (SF) and triplet-triplet annihilation (TTA). K_{q1} and K_{q2} represent the quenching rate constant in the forward (SF) and reverse (TTA) reactions. Figure reproduced from reference.[44].

The SF process can be very fast, similar to other internal conversion processes, especially in molecular crystals, where it occurs on a picosecond or sub-picosecond time scale, competing efficiently with vibrational relaxation and easily occurring effectively at the expense of prompt fluorescence[45]. The process of singlet fission is very promising and can be used to improve the efficiency of solar cells. The singlet fission process can include two chromophores of the same kind (homofission) or chromophores of a different kind (heterofission). Homofission is the type of singlet fission mechanism that will be considered in this thesis.

The energy requirement for singlet fission to occur is $E(S_1 + S_0) \geq 2E\ (T_1)$ from the lowest excited singlet state of bichromophoric molecule or aggregate. This phenomenon is rarely met among light-harvesting materials used in solar cell construction due to relatively small S_1-T_1,

singlet-triplet splittings[19,46]. In addition to the energy requirement, the coupling between the chromophores must be sufficient to aid singlet fission to overwhelm other competing processes, followed by high triplet yield[46,47]. The energy requirement disqualifies most molecules and reduces the set of likely singlet fission chromophores to a small group of materials. However, significant strides have been made in synthesizing derivatives of azulene compounds capable of undergoing a more improved singlet fission process than the azulene itself[47–49].

The $\Delta E(S_2\text{-}T_1)$ in azulene and some of its derivatives are sufficient to allow singlet fission via $S_2 + S_0 \rightarrow T_1 + T_1$ in bichromophoric species, at least on an energy conservation basis[3]. The process of singlet fission generates uncorrelated triplet pairs, which are well separated from each other, resulting from the same spin paired electrons that yield a total magnetic spin (Σm_s) of +1. However, correlated triplet pairs are generated during the intermediate state of the singlet fission process. These correlated triplet pairs can couple with each other effectively to produce a phenomenon known as triplet-triplet annihilation (TTA). TTA is the reverse of singlet fission (see figure 1.8).

Although the possibility of singlet fission from S_2 state in azulene is probable, observation of this process could be hindered because of its shorter T_1 lifetime; $T_1\text{-}S_1$ thermally activated back intersystem crossing is possible and very rapid, and at room temperature, such occurrence is irreversible[19]. However, the fact that aggregates of azulene dimers do not anomalously fluoresce from the S_2 state in low-temperature glasses, as reported by *Ferguson, et al.*, may suggest an effective unrecognized unique singlet fission relaxation process[39]. Under appropriate conditions, azulene derivative compounds such as annulated aromatics, ethene-linked diazulenes, and azulene multimers might also undergo singlet fission from the S_2 state. A typical example is 1,2-benzazulene[50,51]; the $\Delta E(S_0\text{-}S_2)$ energy gap is about twice the excitation energy for T_1. Also, the lifetime for benzazulene is about 74 ps in solution[52], much longer than needed for effective singlet fission in aggregates or linked dimers. Other derivates of azulene synthesized by introducing π-

donating electron groups such as F at odd-numbered position and CN[12] at even-numbered positions of the azulene ring are expected to increase the $S_0 + S_2 \geq 2T_1$ spacing needed to meet the energy requirement for singlet fission to occur. The recent work done by *Wenjun and coworkers* on singlet fission from upper excited electronic states of cofacial perylene dimers brings to light the possibility of singlet fission from the second excited singlet state[53]. We approach this work with a similar focus, investigating the possibility of singlet fission from the second excited state of 1,2-benzazulene, which is a derivative of azulene.

1.6 Motivation for this research

This research work will focus on the photophysical and electronic properties of benzazulene, using azulene for comparison. Azulene's fluorescence from the S_2 state, as suggested by *Reis, e Sousa et al.* undergoes self-quenching with a diffusion-controlled rate constant[1] at dilute concentrations and a static quenching component at higher concentrations. The S_2 self-fluorescence quenching was reported to have resulted from the collisional interaction between azulene molecules, one at the second excited singlet state and the other molecule at the singlet ground state and a short-range energy transfer from an excited azulene molecule to a ground state azulene molecule owing to a significant overlap between the S_2-S_0 fluorescence and S_1-S_0 absorption spectra[1]. The mode of the energy transfer as stipulated in this work is internal conversion via S_2-S_1[1]. The experimental findings reported by *Reis, e Sousa et al.* suggest that the S_2 fluorescence quenching mechanism, which involves energy transfer at a higher concentration range, may also indicate the possibility of a singlet fission process. However, this narrative is not captured by *Reis, e Sousa et al.* as such form one of the bases for our research work. Given this, it will also be advantageous to explore the possibility of self-quenching in concentrated benzazulene samples to understand whether the quenching mechanism proceeds via diffusion-controlled process, static or both (dynamic and static). Also, to date, the process of singlet fission

has not been documented or experimentally proven either in azulene aggregates, its dimers[39] or multimers or even in azulene thin films [54]. However, there are hints in the literature that suggest that singlet fission may occur in azulene aggregates [3,39,45,54] or some of azulene derivative compounds via $S_2 + S_0 \rightarrow 2T_1$ on an energy conservation basis[3]. As such, it is important to investigate the likelihood of singlet fission in concentrated benzazulene samples as its S_2 lifetime is about 74 ps in solution[52], much longer than needed for effective singlet fission process in aggregates or linked dimers. This was an under-developed study as such requires more research and understanding on the spectroscopic and photophysical similarity and differences between azulene and its derivatives, as well as the potential ability of these derivatives to be used as a singlet fission material. This is the primary focus of our study in this thesis.

1.7 Research objectives and hypotheses

Previous findings in the literature have revealed interesting electronic properties of azulene aggregates and its derivatives. Especially the possibility of singlet fission process in azulene aggregates or azulene-derivative compounds. On this bases, the hypotheses to be tested are:

1. The S_2-T_1 electronic energy gaps in azulene and some of its derivatives (1,2-benzazulene) are sufficient to allow singlet fission via $S_2 + S_0 \rightarrow 2T_1$ in bichromophoric species, at least on an energy conservation basis
2. There may be interesting spectroscopical and photophysical similarities and differences between azulene and 1,2-benzazulene, considering that 1,2-benzazulene is a derivative of azulene.

From the hypothesis stated above, the ultimate questions that this research work seeks to answer are; can azulene aggregates or azulene-derivative compounds be used as a singlet fission material? And secondly, what are the possible spectroscopic and photophysical differences and similarities between azulene and its derivative compounds, specifically 1,2-benzazulene? To

answer these questions, solution samples of azulene and 1,2 benzazulene and thin films of 1,2-benzazulene samples were subjected to steady-state absorption and fluorescence measurements. Time-resolved techniques, specifically; Time correlated single photon counting, non-linear fluorescence upconversion and Picoseconds transient absorption spectroscopy, were also employed in this study. The next section will describe in detail the techniques used in investigating the spectroscopy and photophysics of 1,2-benzazulene.

1.8 Techniques employed to study the spectroscopy and photophysics of 1,2-benzazulene

1.8.1 Time-resolved fluorescence

1.6.1.1 Time correlated single photon counting (TCSPC)

TCSPC is a spectroscopic technique used for fluorescence lifetime measurement. The basic principle of TCSPC technique has been the subject of numerous reviews and publications[55,56]. TCSPC measurement involves the detection of a single photon from a fluorescent molecule after an excitation event using a pulse laser source. A significant amount of the emitted single photons are collected after many excitation pulses. From this event, the TCSPC system builds up a probability histogram count versus time channels representing the intensity decay of the sample[55]. The following paragraph will describe the instrumentation and the basic operation principle of the TCSPC technique.

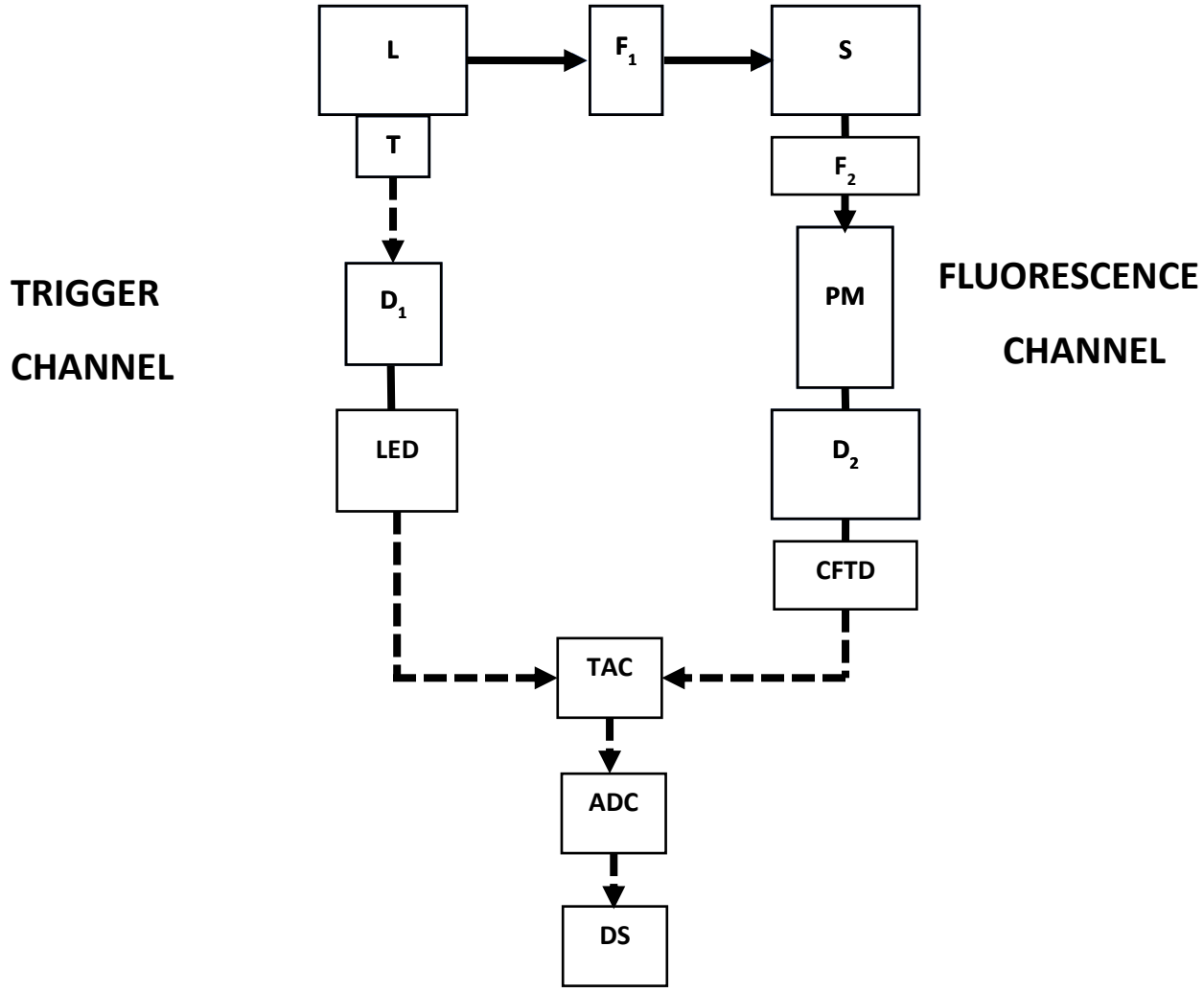

Figure 1.9: A block diagram illustrating the basic principles of how single photon measurements are performed. The solid lines represent optical signal, and the broken lines represent electronic signal; L, indicates the excitation source; T, trigger (photomultiplier tubes); S, sample holder; F_1, F_2 represents filter or monochromator; PM, fast photomultiplier tube; D_1, D_2, delay lines; LED, leading-edge timing discriminator; CFTD, constant fraction timing discriminator; TAC, time-to-amplitude converter; ADC, analogue-to-digital converter; DS, data store which consists of multi-channel analyzer (MCA) or a computer. Figure reproduced from reference.[55].

With regards to the block diagram (see figure 1.9), the experiments begin with the excitation pulse exciting the sample and a trigger, usually a photomultiplier that produces an electrical pulse at a time correlated to the time taken for the excitation source to produce the optical pulse. The pulse generated by the trigger is transmitted through a constant fraction timing discriminator (CFTD) to start the input of the time-to-amplitude converter (TAC), which triggers the voltage ramp in the TAC[42] (START pulse). The excited sample subsequently fluoresces. To ensure that only one emission photon is detected per an excitation event, the photon detection rate

is kept low (usually 5% or lower) in contrast to the rate of the exciting lamp. The voltage ramp from the TAC is brought to a halt once the first photon is detected (STOP pulse). The TAC produces an output pulse whose amplitude is proportional to the voltage and the time difference between the STOP and START pulses[55]. The output pulse from the TAC (voltage) is converted to a time channel by the multi-channel analyzer using the analogue-to-digital converter (ADC)[56]. This process is repeated until about 10,000 counts are collected in the peak channel[42]. In this case, the histogram of the photon's arrival time represents the sample's true intensity decay curve. If deconvolution of the intensity decay curve is required, the time profile for the excitation pulse is measured using a light scatterer to determine the instrument response function (IRF)[56]. The light scatterer may include a dilute colloidal silica or a solvent that does not fluoresce at the excitation wavelength. The IRF represents the shortest time profile that the instrument can measure. This technique is specifically useful in measuring the fluorescence lifetime of azulene which is within the nanoseconds time range.

1.6.1.2 Fluorescence upconversion

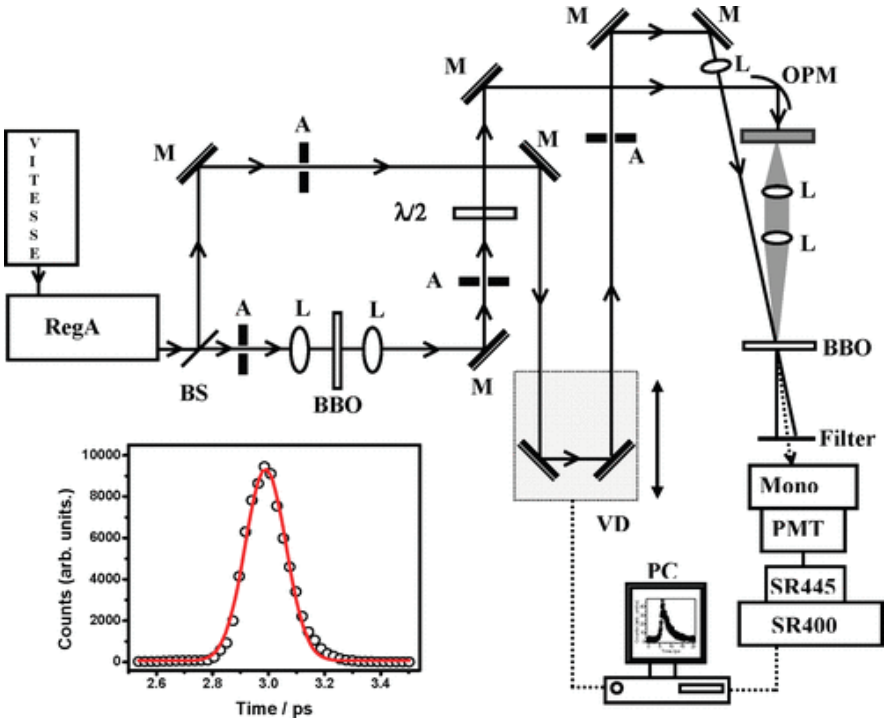

Figure 1.10: A schematic diagram indicating the arrangement of fluorescence upconversion apparatus with cross-correlation trace at the lower-left corner of the figure: BS, beam splitter; L, plano-convex lens; A, aperture; OPM, off-axis parabolic mirror; Mono, monochromator; VD, variable delay. Figure reproduced from reference.[57].

Figure 1.10 represents a schematic block diagram of the fluorescence upconversion set-up. In this technique, the light pulses from a femtosecond or picosecond laser source are amplified with a regenerative amplifier and then split up into two using a beam splitter. One of the two beams is frequency-doubled to generate the pump beam. The other light beam is passed through a delay line and then focused onto the upconversion crystal, which is used as the gate pulse for sum-frequency generation. The pump beam is focused onto the sample using a converging lens for excitation and the subsequent fluorescence emissions produced are collected and focused onto the upconversion crystal. The overlap between the fluorescence signal and the gate pulse leads to a harmonically generated signal with a shorter wavelength known as the upconverted fluorescence signal (see figure 1.12 -blue). The upconverted signal is passed through a filter and an iris to remove all scattered laser light and then directed onto the entrance slit of the monochromator. The

wavelength of the upconversion signal is detected by a photomultiplier placed after the monochromator. The intensity of the up-conversion can be measured as a function of decay time by delaying the moment at which the gate pulse reaches the non-linear crystal and mixes with the fluorescence, as illustrated in Figure 1.11 (down). The upconverted signal is described by the expression

$$\frac{1}{\lambda_{UC}} = \frac{1}{\lambda_{gate}} + \frac{1}{\lambda_{em}} \qquad \text{eqn (1.13)}$$

Where $\boldsymbol{\lambda}_{UC}$ represents the wavelength for the upconverted signal, $\boldsymbol{\lambda}_{gate}$ is the wavelength for the gate pulse and $\boldsymbol{\lambda}_{em}$ is the wavelength at which the fluorescence emission is detected[58]. The fluorescence upconversion technique was important in measuring the fluorescence lifetime of benzazulene which falls within the picosecond time range compared to azulene, whose lifetime is within the nanosecond range hence can be analysed using the TCSPC technique.

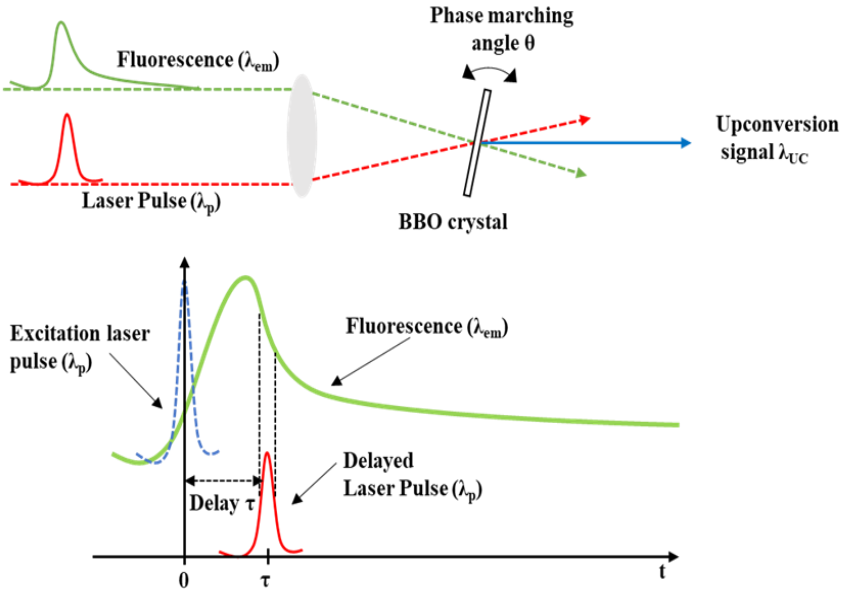

Figure 1.11: A schematic diagram showing the basic principle of operation for fluorescence upconversion technique. The top figure indicates the generation of the upconverted signal (blue) due to the cross-correlation between the fluorescence emission (green) and the laser pulse (red) at

a specific phase-matching angle as the position of the delay stage is being varied (down). Figure Reproduced from reference.[59].

1.6.2 Time-resolved absorbance

1.6.2.1 Transient absorption spectroscopy (TAS)

Transient absorption spectroscopy is a pump-probe spectroscopic technique used to study the details of chemical processes occurring on a picosecond and femtosecond time scale. This technique is particularly useful in investigating singlet fission in azulene and its derivative compounds, where intersystem crossing to the triplet state from the singlet plays a significant role. This technique can be used to study other processes, including energy or electron transfer and vibrational relaxations. These processes can be monitored in real-time using transient absorption spectroscopy. *Wejun, et al.* used this technique to determine the triplet yield of cofacial perylene dimers while studying SF from the upper excited state[53]. Also, *Sundström, et al.*[60], *Van Amerongen, et al.*[61], *Van Grandelle, et al.*[62] have used this technique to investigate the process of energy transfer in photosynthetic membranes. Hence, we intend to study the possibility of singlet fission utilizing this technique.

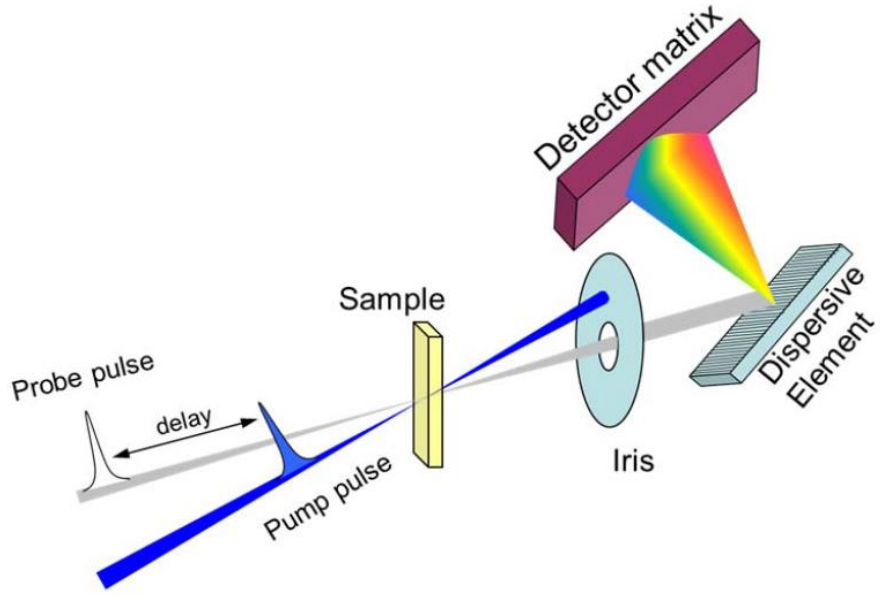

Figure 1.12: A schematic diagram illustrating the principle of operation of transient absorption spectroscopy where the pump pulse (blue) is used to excite the sample and the probe pulse (grey) monitors the sample response at different times. Figure reproduced from reference.[63].

With reference to figure 1.12, the process of transient absorption spectroscopy involves the excitation of a fraction of molecules in a sample using a pump (excitation) pulse generated from a picosecond or femtosecond laser source. A weak probe pulse generated from a portion of the picosecond or femtosecond laser source is passed through the sample relative to the pump pulse with a delay time τ[64]. The probe pulse is usually a low-intensity pulse used to avoid any multistep processes during probing. In this technique, the probe pulse is measured for changes in absorption (ΔA), described by subtracting the absorption spectrum of the sample in the ground state from the absorption spectrum of the excited sample as a function of wavelength and time ΔA ($\boldsymbol{\lambda}$, τ). This is obtained by varying the delay time between the probe and the pump pulse[63]. The change in absorption spectrum (ΔA) contains contributions from different processes, including ground state bleaching, excited state absorption, stimulated emission, and product absorption[63].

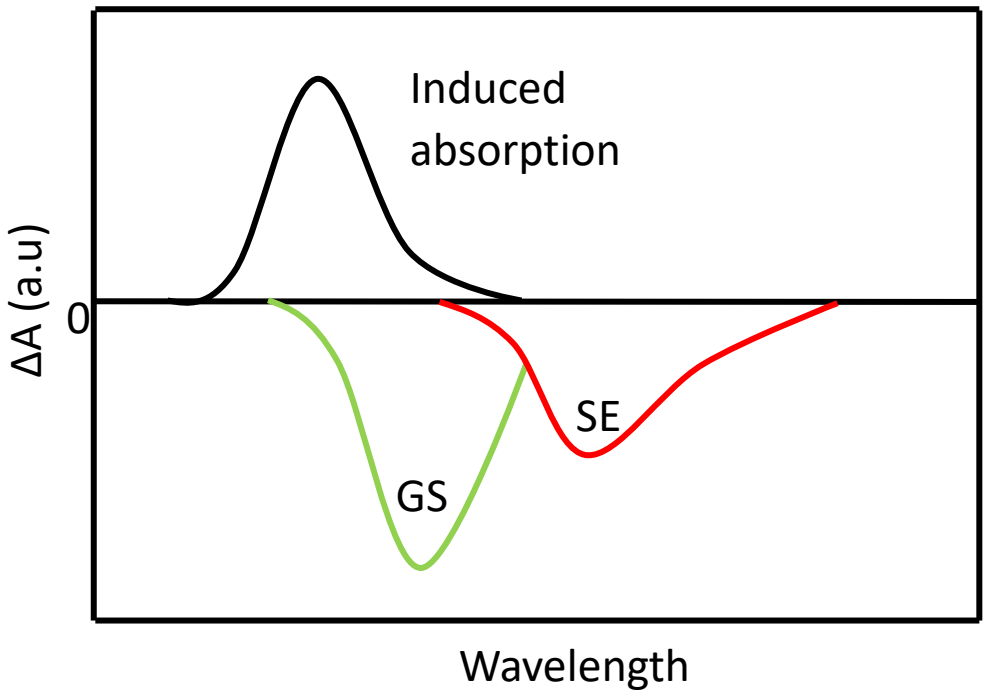

Figure 1.13: Transient absorption spectrum indicating the contributions of different electronic transitions (induced absorption; black, ground state bleach; green and stimulated emissions; red).

Ground state bleach

Excitation of the portion of the sample by the pump pulse to the electronically excited state leads to the reduction of the population in the ground state. The depletion of the ground state population causes the ground state absorption to be less than the absorption of the non-excited sample. This occurrence produces a negative signal in the ΔA spectrum[64], as noticed for the ground state absorption (see figure 1.13 - green).

Stimulated emission.

Stimulated emission is observed when the probe pulse encounters molecules that have been initially excited in the process, inducing fluorescence emission. The spectrum obtained from this process is Stokes shifted relative to the ground state bleach due to the relaxation of the molecule and its immediate environment in the excited state[63] (see Figure 1.13 - red). Emitted photons from the excited molecules as they return to the ground state have identical direction, polarization and wavelength as the photons from the probe pulse that induced it. As such, both photons will be detected with increased overall intensity[63]. This causes the spectrum obtained from the stimulated emission to be similar to the ground state bleach signal (ΔA is negative). In some cases where the Stokes shift for the stimulated emission is very small, the spectra from the ground state bleach and the stimulated emission overlap and are indistinguishable[64].

Induced absorption

Induced absorption occurs when molecules in the excited state move to a higher excited state due to the absorption of the pump beam. This occurrence generates additional absorption and the ΔA obtained from this process becomes positive[63] (figure 1.13-black). Induced absorption is not only noticed for singlet excited state molecules. It can also be observed for molecules that have

undergone intersystem crossing to the triplet state corresponding to $T_1 \rightarrow T_n$ electronic transition where n = 2, 3… etc.

Product absorption

Another contributing factor to the ΔA spectrum is product absorption, where reactions may occur at the excited state, resulting in a long-lived molecular state like the triplet and charge-separation states. The absorption spectrum obtained from this event is associated with a positive signal in the ΔA spectrum[63].

Chapter 2: Spectroscopic measurements of azulene and 1,2-benzazulene

The spectroscopic techniques used for data collection and methods of sample preparation will be described in this chapter. Emphasis will be placed on the details of the time-resolved techniques used in this study to understand the excited state dynamics of the molecules using their lifetime measurements.

2.1 Materials Investigated

The azulene sample (99% purity) was purchased from Sigma-Aldrich and was used as received. The benzazulene sample used in this work was synthesized by our research partners at the University of Melbourne, Australia. Solvents used in preparing all sample solutions include spectroscopic grade toluene (Tol), methylcyclohexane (MCH) and methanol (MeOH), and all were purchased from Sigma-Aldrich.

2.2 Sample preparation and instrumentation

Various concentrations of azulene samples were prepared in MCH. The highest concentration for the azulene sample was 0.1 M, from which 0.0500, 0.0250, 0.0125, 0.0063, 0.0032 and 0.0016 M were made by diluting an aliquote of the 0.1 M concentrated azulene solution. For the 1,2-benzazulene samples, 10 mM, 700, 350, 139, 50 and 25 μM concentrations were prepared in MCH for absorption, fluorescence and time-resolved measurement. Also, 50 μM of 1,2-benzazulene in toluene, methanol and methylcyclohexane were prepared for steady-state absorption measurement in order to compare and investigate the effect of solvent on their various absorption bands. In addition, very dilute concentrations (10 and 25 μM) of azulene and benzazulene in MCH and Tol were prepared to compare their absorption, fluorescence, and lifetime spectra with those of the higher concentrations for evidence of aggregation if formed. The

samples were stored in a fridge in paraffin-taped vials to avoid solvent evaporation. All measurements were made at room temperature.

Benzazulene thin film preparation

For the film preparation, 10 µL of 10 mM 1,2-benzazulene solution in MCH was deposited twice onto a clean 25 x 25 mm quartz disc purchased from Edmund optics to form 2 layers. For each layer, the solid thin film was allowed to air dry before depositing the next layer. The ready-prepared thin film was subjected to steady-state absorption and fluorescence measurements.

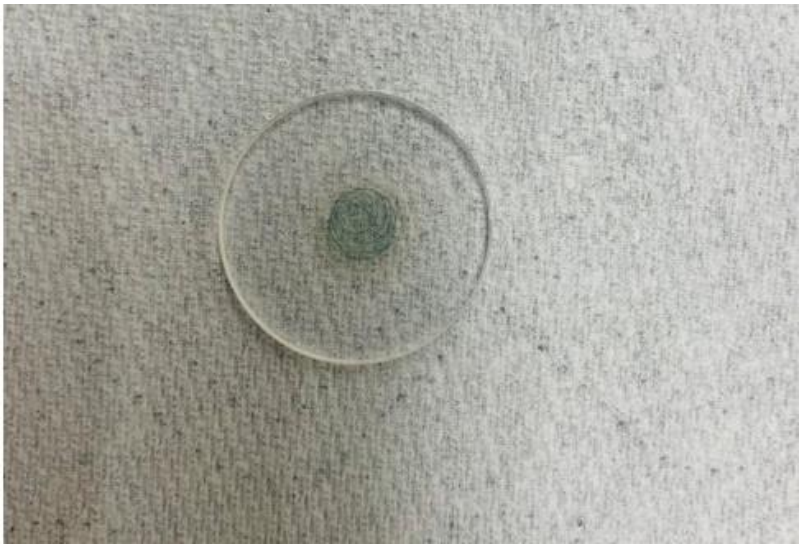

Figure 2.1: A pictorial view of the drop-casted 1,2-benzazulene (2-layers) thin film on a quartz disc.

2.2.1 Steady-state absorption and fluorescence measurements

A photochemical decomposition experiment was carried out to determine the extent to which the 1,2-benzazulene sample will be degraded when exposed to a laser light source. This measurement was carried out over one hour by continuously exciting a vigorously-stirred 105.5 µM benzazulene in toluene solution with a 355 nm laser at 5.14 mW power. The amount of power absorbed by the 10 mm pathlength of the sample was 2.34 mW. The decomposition was monitored at 403 nm wavelength by measuring the sample's absorption at 10 or 20-minute intervals with a Cary 6000i dual-beam spectrophotometer. The photodecomposition quantum yield was calculated

by taking the ratio of the number of molecules that decomposed per total time and the number of photons absorbed (see Appendices – additional calculations). In addition, the absorbance spectra of the various samples, i.e. 50 µM benzazulene in toluene, methanol and methylcyclohexane, and 10 µM azulene in toluene, were measured using the same Cary 6000i spectrophotometer. 10 mm cuvette was used for the spectroscopic measurements. But for highly concentrated samples, 0.1 mm pathlength quartz cuvette was used for the absorbance measurements.

Steady-state fluorescence emission measurements were carried out on the same sample solutions by means of a standard PTI QuantaMaster double-monochromator fluorometer with excitation and detection slit widths of 1.5 mm and 3.0 mm, respectively. A custom-modified SPEX fluorometer with excitation lasers at 355, 405, and 561 nm coupled with a set of neutral density filters was used to reduce the amount of laser power reaching the sample to avoid sample decomposition. Notch filters were used to eliminate scatter from the exciting lasers. Also, a 520 nm long-bandpass filter was placed at the emission pathway to differentiate between a second-order diffraction peak of S_2 fluorescence from any actual S_1 fluorescence. At 355 nm excitation, a 1 mm slit width was used, and at 405 and 561 nm excitation, a 3 mm slit width was used for the fluorescence measurements. All fluorescence spectra were tested in 2 mm x 10 mm rectangular cuvettes for the 1,2-benzazulene samples, whereas a triangular cuvette was used for the concentrated azulene samples to avoid reabsorption of fluorescence emission.

2.2.2 Time-correlated single-photon counting (TCSPC) measurements.

The azulene solution samples were excited using Ti/sapphire laser (Coherent Mira 900F/APE pulse switch) pumped by a Coherent Verdi laser. The laser output (930 nm wavelength, 4.7 MHz repetition rate) was frequency-tripled to provide an excitation into the S_2 state of azulene at 310 nm wavelength. The emitted photons were detected at 375 nm wavelength, the maximum fluorescence peak observed in the steady-state fluorescence measurement of azulene. The

individual fluorescence decay curves were collected after transmission through an emission polarizer accurately positioned at the magic angle and then through a monochromator. The signal was detected by a multi-channel plate-photomultiplier tube (R3809U-51, Hamamatsu) which was then fed to a time-correlated single-photon counting (TCSPC) module. The data was collected using SPC-830 Software (Becker and Hickl). The fluorescence lifetime of azulene from the S_2 state is extracted from the decay profile using Psdecay2000 software. This software performs a deconvolution of the decay file from a scattered light file via an iterative reconvolution. The instrument response function was measured using scattering from methylcyclohexane with the detection and excitation wavelength set at 310 nm. The FWHM obtained from this measurement was 0.031ns

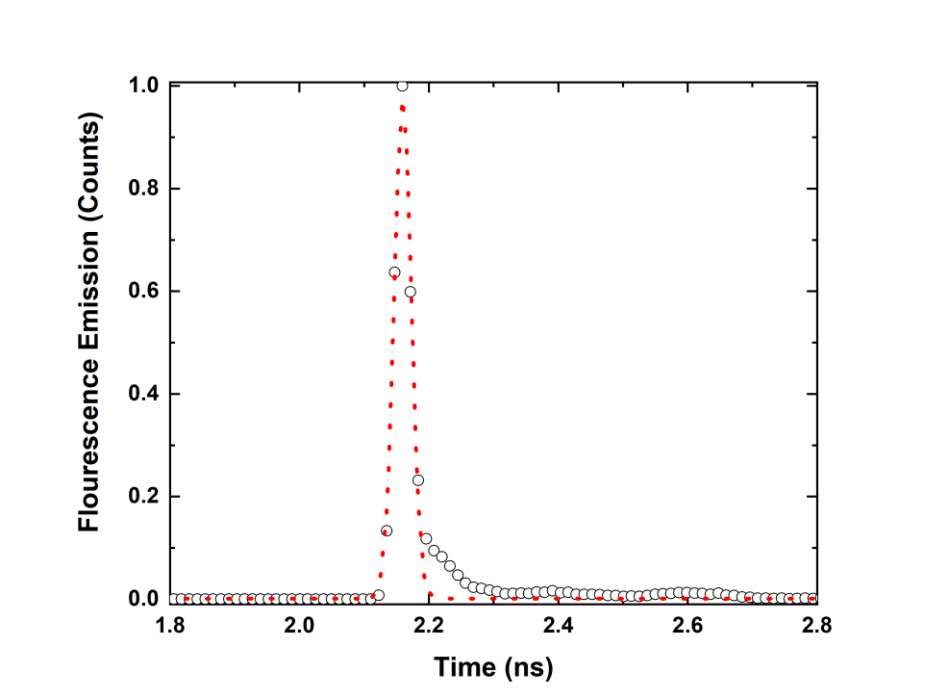

Figure 2.2: The fitted curve (red) and instrument response function (black circles) of the excitation pulse obtained from the TCSPC system, measured using a light scatterer, methylcyclohexane. The estimated FWHM was 0.031 ns. The excitation and emission wavelength was 310 nm

2.2.3 Non-linear fluorescence upconversion measurement (UC)

In this study, a femtosecond Ti-Sapphire laser (Coherent Vitesse duo) amplified by a regenerative amplifier was used. The laser output power and wavelength were 37.7 mW and 800 nm, respectively. The detection wavelength for this measurement was set at 435 nm, close to the S_2 fluorescence emission peak of 1,2-benzazulene coupled with a 10 kHz laser repetition rate. With a beam splitter, the output from the Reg A was divided into 80/20 %. The 20% beam light generated from the Reg A output was used to produce the second harmonics of the pump beam. The 80 % was passed through a variable delay line and focused onto an upconversion crystal (BBO crystal), which served as the gate pulse for sum-frequency generation. The second harmonic generation was obtained by passing the 20 % of the Reg A output through a thick type I BBO crystal at a specific phase-matching angle. The pump beam was focused onto the 1,2-benzazulene sample for excitation while continuously stirring the sample in a 2 x 10 mm quartz cuvette. The emitted fluorescence was collected and focused onto an upconversion crystal using a collimating lens. The overlap between the fluorescence signal and the gate pulse in the BBO crystal yields a harmonically generated upconverted fluorescence signal. The upconverted signal was passed through a filter and an iris to remove all scattered laser light and then directed onto the entrance slit of the monochromator. The wavelength of the upconversion signal was detected by a photomultiplier placed after the monochromator. The intensity of the up-conversion was measured as a function of decay time by delaying the moment at which the gate pulse reaches the non-linear crystal and mixes with the fluorescence. The instrument response function for this set-up was 380 fs (FWHM) obtained using the Raman peak of toluene centred at 462.5 nm as a guide. In this measurement, it was ensured that the count rate for the upconverted fluorescence peak was limited to $\leq 5\%$ of the laser's repetition rate. This is ensured to eliminate photon-counting artifacts resulting from detection electronics.

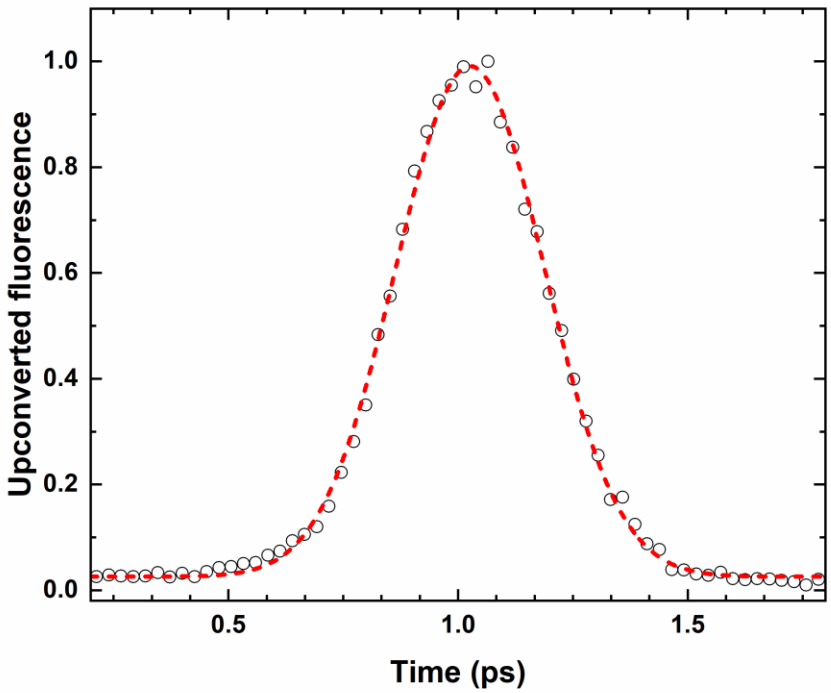

Figure 2.3: The fitted curve (red) and instrument response function (black circles) of the non-linear fluorescence upconversion system measured using Raman scattering from spectroscopic grade toluene at a detection wavelength of 462.5 nm. The FWHM was 380 fs

2.2.4 Transient absorption measurement

The transient absorption measurements for the 1,2-benzazulene were performed by our collaborators at the University of Melbourne, Australia. The transient absorption spectra of the 1,2-benzazulene samples with their corresponding decay and temporal rise curves were obtained with a 400 nm excitation laser and a delayed supercontinuum probe light with an estimated IRF of 150 fs FWHM.[65]

Chapter 3: Results and Discussion

In this chapter, it is important to mention that some of the work presented in this thesis has been published. It is referenced in this thesis with reference number 74.

3.1 Aggregation studies of azulene

3.1.1 Steady-state absorption and fluorescence

This thesis aims to investigate the spectroscopy and the photophysics of 1,2-benzazulene using azulene for comparison. However, it is important to first understand the spectroscopy and the photophysics of azulene. The spectroscopic property and the photophysics of azulene have been significantly reported in the literature.[1,2,16,19,28,39,66–71]. Figure 3.1 shows the absorption spectra of the various concentrations of the azulene sample in methylcyclohexane (MCH).

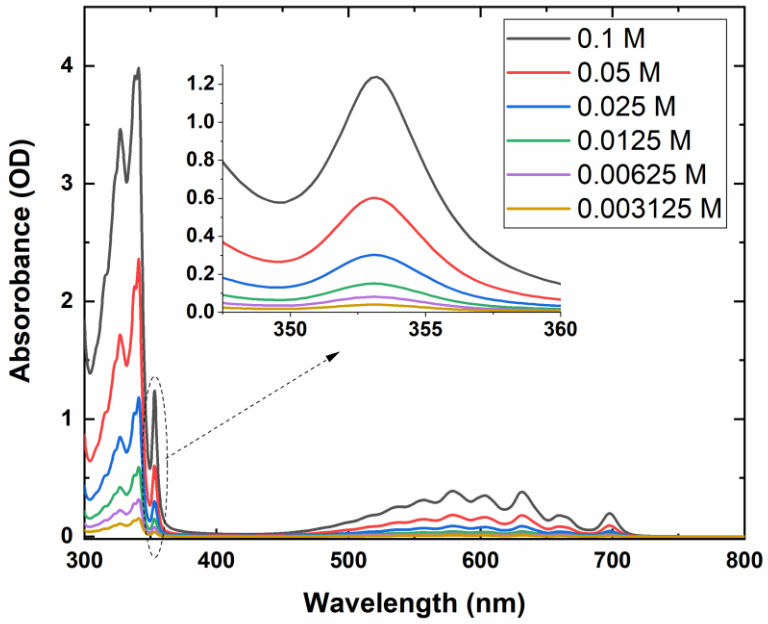

Figure 3.1: Absorption spectra of the various concentrations of azulene in MCH indicating the S_1 and S_2 regions. The inset is the enlargement of the S_2-S_0 region displaying the origin band (0-0).

The weak absorption bands around 500 – 777 nm correspond to the S_1 state with the origin band, S_1-S_0 (0-0), at 698 nm. The 353 nm strong absorption band is assigned to the S_2 state. The higher bands at 341 and 326 nm could be assigned to higher electronic transitions to the S_3 and S_4 states similar to that reported by *Ferguson, et al.*[39]. As the concentration increases, the absorbances increase. However, there is no change in the spectra shape or significant spectral shift associated with any of the samples as observed on the normalized absorption spectra plot. This occurrence is indicative of no formation of aggregates in liquid solution in agreement with that reported by *Reiss, et al.* [1]. A linear absorbance plot as a function of concentration gave a nearly perfect straight line through the origin, confirming the absence of aggregation in the azulene samples (see Figure 3.2B) consistent with Beer Lambert's law. However, there is evidence of aggregation documented by *Ferguson, et al.*[39] in the $S_0 \rightarrow S_2$ absorption region when studying the spectra of azulene dimers at low temperature (77K) in an organic glassy matrix. To understand the $S_2 \rightarrow S_0$ electronic transition and the anti-Kasha property of azulene, the following paragraph will describe the fluorescence spectra of azulene and its electronic properties.

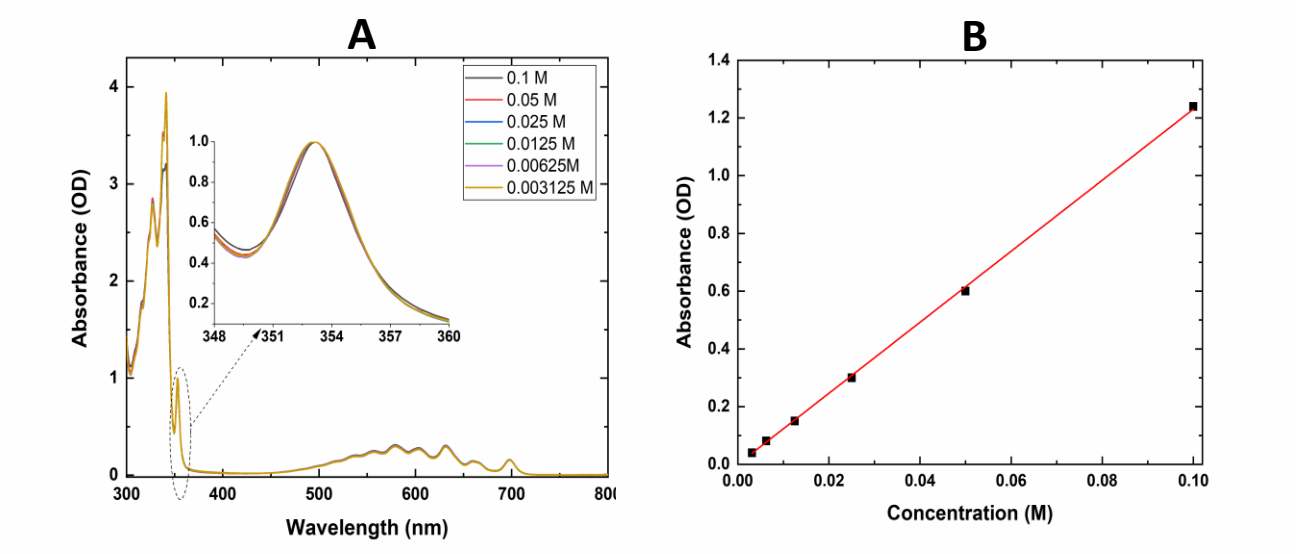

Figure 3.2: A: Absorption spectrum of various concentrations of azulene in MCH normalized at 353 nm. The inset shows the spectra for the S_2-S_0 regions, indicating no obvious evidence of aggregation. **B:** Linear absorbance plot of azulene at 353 nm against concentration. The perfect straight line through the origin of the plot also indicates no obvious evidence of aggregation.

From the fluorescence spectra, the anomalous fluorescence emission centred at 375 nm is assignable to the S_2 of azulene in agreement with that described in the literature[1,2,28,34,39,69,71]. This unusual fluorescence emission from the S_2 state was reported to have resulted from the large energy gap between the S_1 and S_2 states. This large energy gap disfavors the intersection of potential energy surfaces, and produces a small S_2-S_1 Franck-Condon factor, rendering radiationless transitions from the upper to the lower state ($S_2 \rightarrow S_1$) improbable. Hence, the anti-Kasha fluorescence decay from $S_2 \rightarrow S_0$ becomes a more likely transition. Also, no $S_1 \rightarrow S_0$ fluorescence emission was observed from our fluorescence spectra. This was previously documented[2,34,72] to have resulted from the conical intersection of the potential energy surfaces of the S_1 and S_0 state. The conical intersection between the S_1 and S_0 states creates a path for an efficient repopulation of the ground state via vibrational relaxation. This radiationless decay is an ultra-fast process that outcompetes fluorescence emission. Also, there is no spectral change associated with the fluorescence spectra with varying concentrations. This occurrence eliminates the possibility of other excited state fluorescent species being formed. However, the fluorescence emission intensity decreases as the azulene concentration increases. This occurrence is indicative that $S_2 \rightarrow S_0$ azulene fluorescence is self quenched, as indicated in Figure 3.3. This observation is in agreement with the findings reported by *Reis, et al.*[1]. The details of the S_2 fluorescence quenching mechanism are explored using time-resolved measurement. The S_2 fluorescence lifetime of azulene is measured and monitored as a function of varying concentration using TCSPC technique. The following paragraph will discuss how the S_2 fluorescence lifetime of azulene decreases as the concentration increases, indicating S_2 fluorescence quenching.

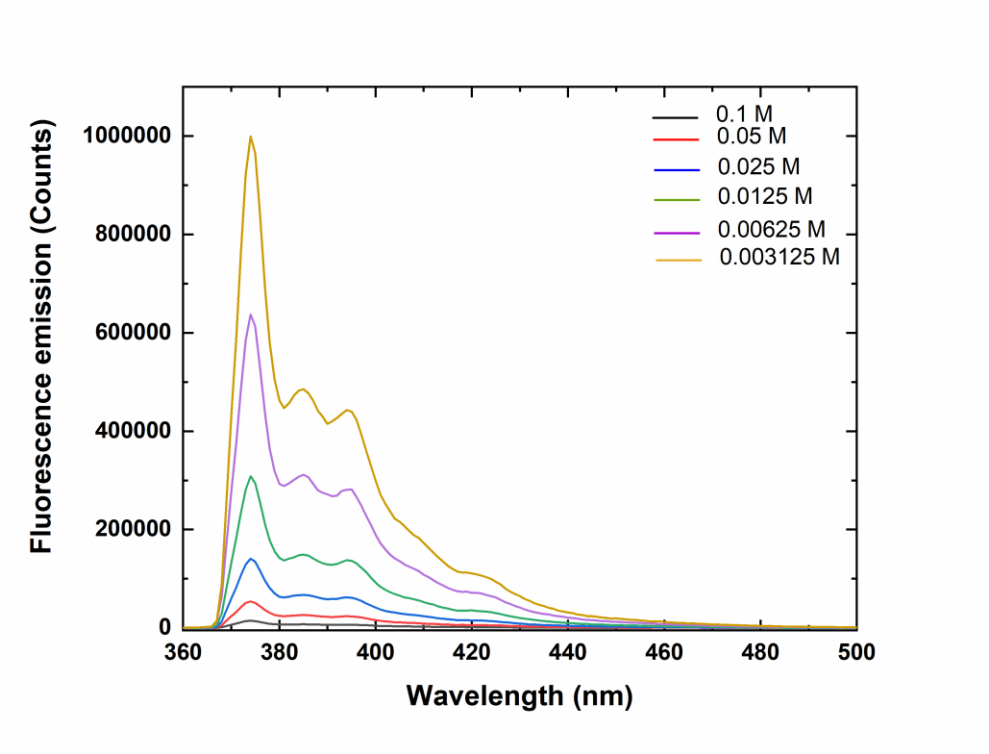

Figure 3.3: Azulene fluorescence from the S_2 state showing the reduction of fluorescence intensity as concentration increases. Spectra background and absorbance corrected. The excitation wavelength was 355 nm with 14.5 mW laser power obtained with 3,3 neutral density filters in place. A 355 nm notch filter was positioned at the emission pathway with a 1 mm slit width. The samples were prepared in MCH.

3.1.2 Time correlated single-photon counting (TCSPC) measurements

To understand the photophysics of azulene, the self-quenching mechanism of azulene from the S_2 state was monitored using time-resolved measurement. The decay curve was fitted with a single exponential function (see eqn 1.6) to obtain the S_2 lifetime of the various concentrations. It can be noticed from figure 3.4 and table 1 that the S_2 lifetime decreases as the concentration increases, following a similar trend as the fluorescence emission measurement.

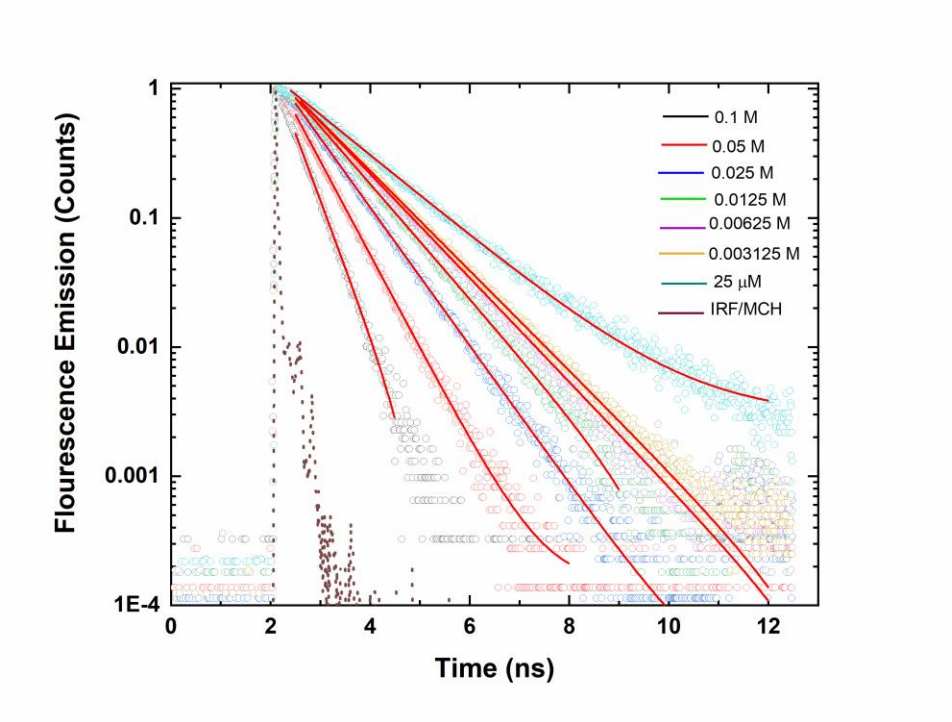

Figure 3.4: S_2 fluorescence lifetime decay measurement of various concentrations of azulene in MCH using TCSPC, showing the decrease in S_2 fluorescence decay as concentration increases. The decays were fitted using a single exponential decay function. The samples were excited at 310 nm and detected at 375 nm using a 2 x 10 mm cuvette. The instrument response function was estimated to be 0.031 ns.

Table 1: Table of values showing the S_2 lifetime obtained for each azulene sample in MCH using TCSPC. The fluorescence decay profiles were fitted using Origin software.

Concentration (mol/L)	**Lifetime (ns)**
0.1	0.404 ± 0.011
0.05	0.590 ± 0.009
0.025	0.799 ± 0.005
0.0125	0.955 ± 0.006
0.00625	1.059 ± 0.007
0.00313	1.130 ± 0.004
0.00156	1.158 ± 0.005
0.00078	1.179 ± 0.004

To describe the details of the quenching mechanism, the Stern-Volmer kinetic equation is used, where k_q represents the time-dependent diffusion rate constant (see eqn 1.12). *Rice and coworkers* reported that for a diffusion-controlled process, the quenching rate coefficient is time-dependent[41]. However, the time dependency of this process is not noticeable on the decay curve analysis but very evident on the Stern-Volmer plot using the ratio of fluorescence intensity in the absence and presence of a quencher at dilute and higher concentrations (see eqn 1.12). This evidence is characterized by an upward curvature in the Stern-Volmer quantum yield plot which is similar to that obtained from our experimental findings, as illustrated in figure 3.5 (right). The upward curvature of the Stern-Volmer plot suggests that the S_2 fluorescence quenching in azulene is not only diffusion-controlled, as shown in figure 3.5 (left) but also associated with a static quenching component at higher concentrations, illustrated in figure 3.5 (right). These findings agree with that obtained by *Reis e Sousa, et al.,*[1] *Rice et al.,*[41] *and Andre, et al.*[73]. The Stern-Volmer plot obtained from the ratio of lifetime measurement as a function of azulene concentration shows that the quenching mechanism of azulene from the S_2 state is diffusion-controlled with a time-dependent diffusion rate constant (k_q) of 1.5×10^{10} $M^{-1}s^{-1}$ at dilute concentrations as suggested by *Reis e Sousa, et al.*[1].

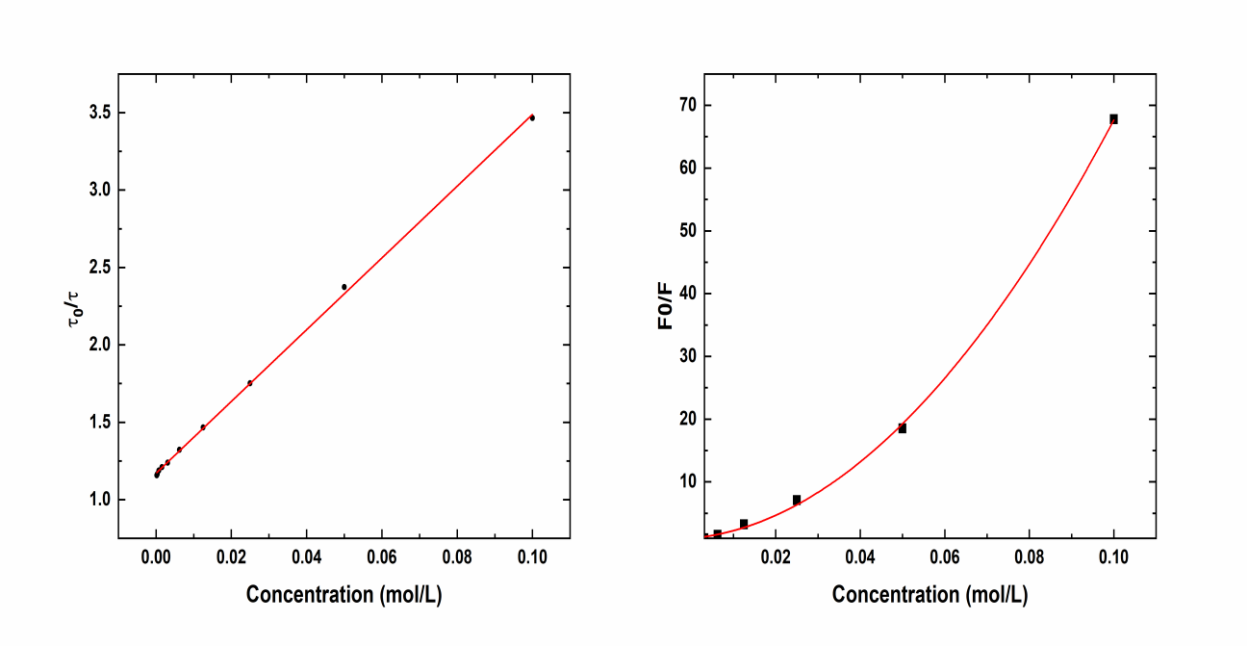

Figure 3.5: Stern-Volmer plot of τ_0/τ as a function of concentration, τ_0 = 1.4 ns, $\boldsymbol{\lambda}_{exc}$ = 310 nm, $\boldsymbol{\lambda}_{emm}$ = 375 nm (left) and Stern-Volmer plot obtained by plotting the ratio of fluorescence quantum yield versus concentration (right).

The quenching mechanism was previously reported[1] to have resulted from an encounter between two azulene molecules, one in its second excited singlet state and the other in the ground state. The interaction between these two azulene molecules yields an efficient fluorescence quenching process which is diffusion-controlled[1]. The absence of evidence of newly formed excited state species and ground state complexes observed from the steady-state absorption and fluorescence measurements suggests that the collisional quenching mechanism results from energy transfer between the excited state and ground state azulene molecules upon the encounter[1]. Also, at higher concentrations, the molecules are fairly close to each other without any contact. The close proximity of these molecules causes a rapid energy transfer from the excited molecule to the ground state molecule. The energy transfer is an ultra-fast radiationless process that outcompetes fluorescence emission. This occurrence constitutes the static component of the fluorescence self-quenching in azulene from the S_2, shown as an upward curvature in figure 3.5 (right) at a higher concentration. The static quenching mechanism was then described to proceed via a short-range radiationless energy transfer from $S_2 \rightarrow S_1$ resulting from the significant overlap between the

$S_0 \rightarrow S_1$ absorption spectrum and the $S_2 \rightarrow S_0$ fluorescence spectrum of azulene[1]. Our experimental result is in agreement with that suggested by *Reis e Sousa and coworkers*[1]. However, we disagree with the proposed quenching mechanism of the azulene fluorescence from the S_2 state. Our experimental findings clearly suggest that the proposed overlap between the S_2 ($S_2 \rightarrow S_0$) fluorescence spectrum and the S_1 ($S_0 \rightarrow S_1$) absorption spectrum of azulene is not significant, as reported by *Reis e Sousa, et al.*[1], on the basis that the fraction of area covered by the $S_2 \rightarrow S_0$ fluorescence spectrum relative to $S_0 \rightarrow S_1$ absorption spectrum is very small (see Figure 3.6) and can be said to contribute partly to the quenching mechanism observe in azulene from the S_2 state. The absence of $S_1 \rightarrow S_0$ fluorescence emission as observed on the fluorescence spectra in figure 3.3 suggests that a radiationless process is occurring at the expense of fluorescence emission. This radiationless process results from internal conversion via $S_1 \rightarrow S_0$ due to the conical intersection of the potential energy surfaces of the S_1 and S_0 state[2,19,66,72]. This occurrence makes it possible for radiationless decay to happen at the expense of fluorescence emission. On this basis, one can conclude that the quenching mechanism of azulene from the S_2 state does not only result from short-range non-radiative energy transfer from $S_2 \rightarrow S_1$ as suggested by *Reis e Sousa, et al.* [1], but $S_1 \rightarrow S_0$ radiationless process also contributes to the fluorescence self-quenching of azulene from the S_2 state.

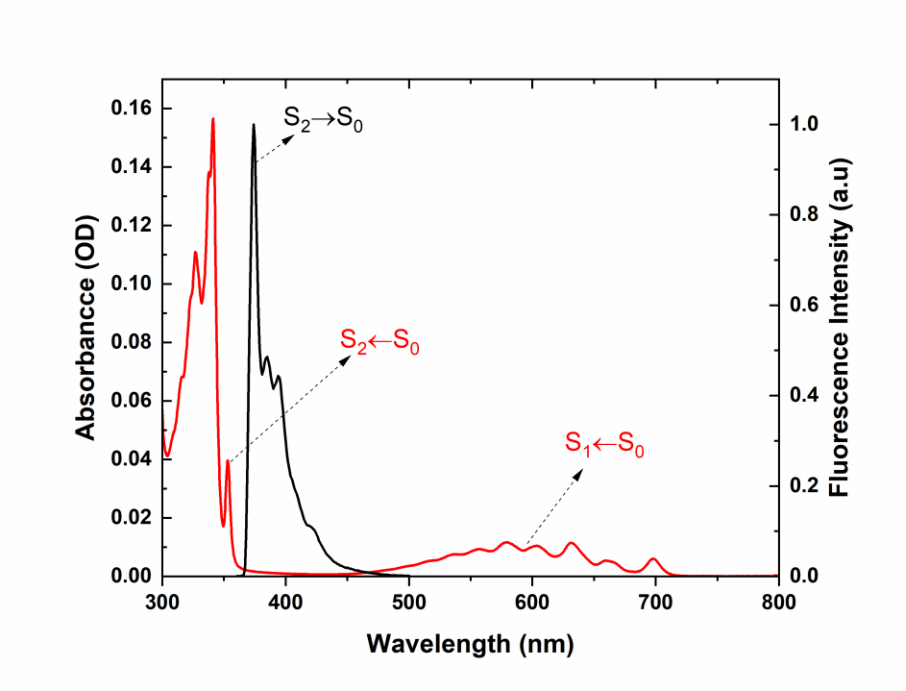

Figure 3.6:Absorption (red) and $S_2 \rightarrow S_0$ fluorescence (black) spectra of azulene in MCH displaying the negligible overlap between the $S_2 \rightarrow S_0$ fluorescence and the $S_0 \rightarrow S_1$ absorption spectra.

3.2 The spectroscopy and photophysics of 1,2-benzazulene compared to azulene

Having understood the spectroscopy and the photophysics of azulene, this research work will now be extended to investigate the spectroscopy and photophysics of 1,2-benzazulene using azulene for comparison. In the study of 1,2-benzazulene, the first reasonable step to take is to determine the extent to which the 1,2-benzazulene sample will be degraded when exposed to a cw laser light source. To examine the photostability of the 1,2-benzazulene sample, a photochemical decomposition experiment was carried out on the sample in aerated toluene and its S_2-S_0 absorbance changes were monitored at 403.5 nm over one hour period. From figure 3.7, it can be noticed that the decrease in the absorbances over the one-hour period is very minimal with a calculated photochemical decomposition quantum yield of 1×10^{-4}. The decomposition experiment suggests that the 1,2-benzazulene sample is stable when exposed to laser light. Given this, one can

then conclude that the photochemical degradation of the benzazulene is not a problem that would affect our experimental measurements.

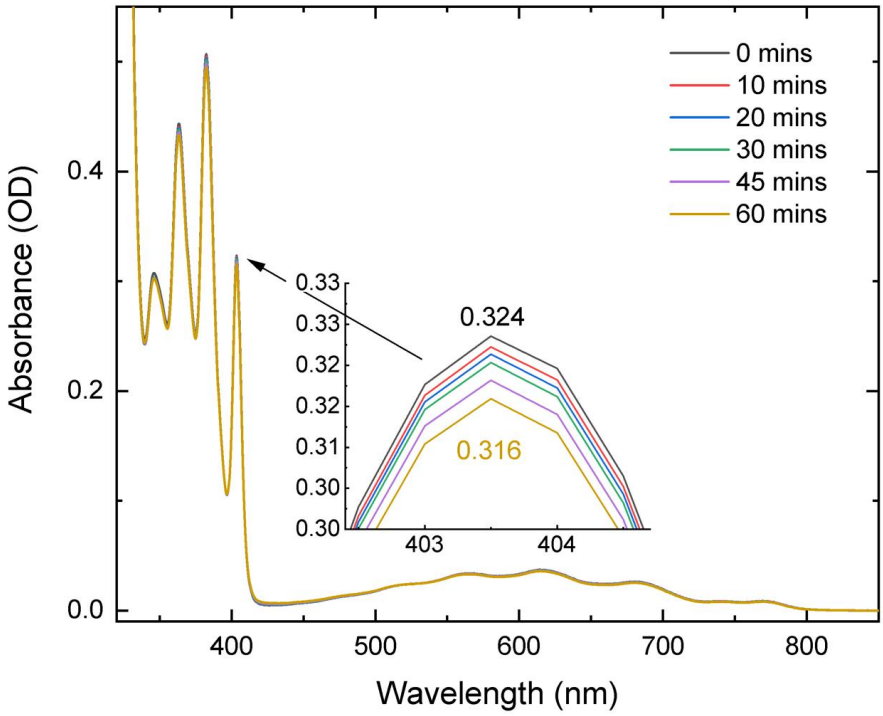

Figure 3.7: Normalized absorption spectrum of 105.5 µM benzazulene in aerated toluene to determine the photochemical decomposition quantum yield over 1 hour, monitored at 403.5 nm. The excitation wavelength was 355 nm. The amount of power absorbed was 2.8 mW and a 1 cm path length cuvette was used. Figure A reproduced from the SI of reference[74]

3.2.1 Spectroscopy

This section discusses the electronic properties of 1,2-benzazulene and the spectroscopic similarities and differences between 1,2-benzazulene compared to its parent molecule, azulene. Figure 3.8A brings to light the effect of solvent (MCH, MeOH and Tol) on the absorption spectrum of 1,2-benzazulene. It can be observed that the shape of the S_1-S_0 and S_2-S_0 absorption bands looks similar and are in agreement with the absorption spectra obtained when the molecule was first synthesized[51,75]. However, in MCH, the S_1-S_0 and S_2-S_0 absorption bands show a vibronically-resolved spectrum compared to the spectra in other solvents, with an S_1 (0-0) origin band at 776 nm. The similarity of the absorption bands in all the solvents coupled with no spectral shift reveals

the absence of ground state aggregation at this concentration (50 µM). However, when a solid thin-film of 1,2-benzazulene (see chapter 2.2) was subjected to absorption measurement, the S_2-S_0 absorption bands were broad and shifted to a longer wavelength relative to the dilute concentration indicative of the formation of ground state aggregation (see figure 3.8B). The formation of this aggregate suggests the possibility of singlet fission in 1,2-benzazulene thin film, as previously reported by *Ferguson, et al.*[39]

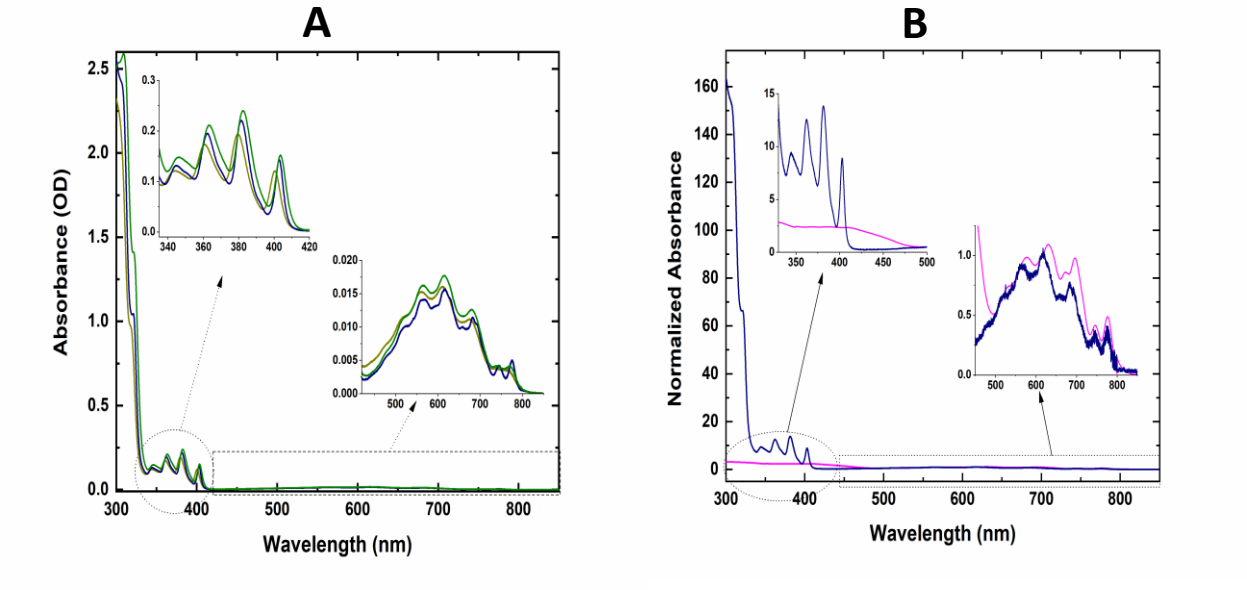

Figure 3.8: A: Absorption spectra of 50 µM 1,2-benzazulene in different solvents; methanol (dark yellow), methylcyclohexane (navy blue) and toluene (olive green). **B:** Absorption spectra of 50 uM 1,2-benzazulene in methylcyclohexane (navy blue) and 2 layers of 1,2-benzazulene thin film (magenta), all normalized at 615 nm for comparison. The inserts on both graphs show the spectra for the S_1-S_0 (right) and S_2-S_0 regions (left). Figure A reproduced from reference[74]

The absorption spectra of azulene and 1,2-benzazulene are shown in figure 3.9 for comparison. It can be observed that the S_1-S_0 absorption bands that corresponds to azulene[76,77] are also present in 1,2-benzazulene. These bands look similar in shape and are relatively weak in intensity compared to the S_2-S_0 absorption band. For 1,2-benzazulene, the oscillator strength, which describes the strength and the allowedness of electronic transition, was determined for $S_0 \rightarrow S_1$ and $S_0 \rightarrow S_2$ using the absorption spectrum. The ratio of the oscillator strength for the S_1-

S_0 and S_2-S_0 absorptions (f_{S2}/f_{S1}) was 13:1, suggesting that $S_0 \rightarrow S_2$ electronic transition are more favourable than $S_0 \rightarrow S_1$ transition.

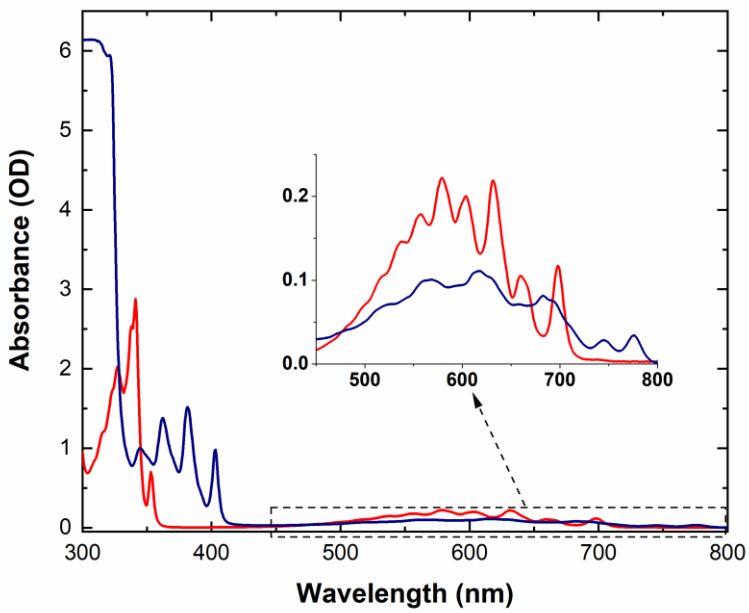

Figure 3.9: Absorption spectra of 0.01 M azulene (red) and 1,2-benzazulene in MCH (navy blue) normalized at 345 nm for comparison. The insert shows the absorption bands for the S_0-S_1 region.

The weak S_1-S_0 absorption bands of 1,2-benzazulene look similar to that of azulene, as shown in figure 3.9. These weak absorption bands result from the polarization along the molecule's short axis[19] and the unsymmetrical arrangement of the frontier orbitals in the S_0 and S_1 state of the azulene moiety. This unsymmetrical arrangement of the HOMO–LUMO decreases the repulsive interaction between the two unpaired electrons. The net effect of these occurrences is the narrowing of the energy gap spacing between the S_1-S_0 absorption spectrum. As a result, azulene tends to absorb weakly in the visible region[19,28]. Given this, it can be concluded that the annelation of azulene with the benzene ring does not significantly change the first absorption band of the 1,2-benzazulene compared to azulene, as illustrated in figure 3.9 above. An exception to this phenomenon is the S_2-S_0 absorption bands. Unlike azulene, the S_2-S_0 absorption spectrum of 1,2-benzazulene exhibits distinct vibrational structures with a strong S_2-S_0 origin band. The vibrational

spacing from v' = 0 to v' = 3 (Franck-Condon series) are approximately equal. (See table 2). The equal vibrational spacing is due to the fusion of the azulene ring to the benzene ring. Table 2 below shows the vibronic frequency calculation of 1,2-benzazulene obtained from the absorption spectra. The values are reported in wavenumber (per cm) even though all the graphs are in wavelength (nm) in order to describe the vibronic frequency of 1,2-benzazulene.

Table 2: The vibronic frequency calculation of 1,2-benzazulene in MCH obtained from the S_2-S_0 absorption spectrum.

Peak # Absorption S_2	**λ (nm) Absorption S_2 (± 0.1)**	**$\bar{\nu}$ /cm Absorption S_2 x 10^2 (± 0.1)**	**($\bar{\nu}$ -$\bar{\nu}_{(0-0)}$)/cm Absorption S_2 x 10^2 (± 0.1)**	**Equal ($\bar{\nu}$-$\bar{\nu}_{(0-0)}$)/cm Spacing S_2**
1	402.8	248.3	0.0	–
2	381.7	262.0	137.2	$\bar{\nu}_1$
3	362.3	276.0	277.5	$2\bar{\nu}_1$
4	344.8	290.0	417.6	$3\bar{\nu}_1$

Also, it can be noted that the S_1-S_0 and S_2-S_0 absorption bands in 1,2-benzazulene are shifted to a longer wavelength compared to azulene. This redshift results from an increase in the larger pi-system of the 1,2-benzazulene ring due to the annelation of benzene to the azulene ring. Table 3 below shows the vibronic origin bands of 1,2-benzazulene expressed in wavenumbers, which are shifted to a longer wavelength compared to azulene. The S_2 – S_1 electronic energy gaps in MCH, MeOH and Tol are also shown in table 3.

Table 3: Data obtained from the absorption spectra of 1,2-benzazulene in MCH, MeOH and Tol showing the energies of the S_2 and S_1 states and its red-shifts relative to azulene

solvent	E(S_1) origin, cm^{-1}	E(S_2) origin, cm^{-1}	$\Delta E(S_2 - S_1)$ cm^{-1}	E(S_1)(Az-1,2-BzAz) cm^{-1}	E(S_2)(Az-1,2-BzAz) cm^{-1}
MCH	12883	24826	11943	-	-
toluene	12998	24784	11786	1437	3502
methanol	13068	24976	11908	-	-

Table of values reproduced from reference.[74]

It was documented by *Vossköter, et al.*[78] that the S_1-T_1 electronic energy gap for azulene is approximately 500 cm^{-1}. Since 1,2-benzazulene is a derivative of azulene, it can be assumed that its S_1-T_1 electronic energy gap is similar to 500 cm^{-1}. The calculation below shows that the energy requirement for singlet fission via $S_2 + S_0 \rightarrow 2T_1$ in 1,2-benzazulene is satisfied.

$$\Delta E(S_1 - T_1) = 500\ cm^{-1}$$

$$E(S_1) = 12883\ cm^{-1} \text{ from table 3}$$

$$\Rightarrow E(T_1) = E(S_1) - \Delta E(S_1 - T_1)$$

$$E(T_1) = (12883 - 500)\ cm^{-1}$$

$$E(T_1) = 12383\ cm^{-1}$$

$$\Rightarrow E(T_1) \text{x } 2 = 12383\ cm^{-1} \text{ x } 2 = 24766\ cm^{-1} \approx 24826\ cm^{-1} = \Delta E(S_2 - S_0)$$

Given this, one can propose that the $\Delta E(S_2$-$S_0)$ is almost equal to $2E(T_1)$ in 1,2-benzazulene hence, the occurrence of the singlet fission process via $S_2 + S_0 \rightarrow 2T_1$ should be almost thermoneutral.

The Figure 3.10 below (left) shows the S_2-S_0 fluorescence spectrum of 1,2-benzazulene in toluene excited at the S_3-S_0 origin band (320 nm) with azulene for comparison. Like azulene, 1,2-benzazulene molecule emits anomalous fluorescence from the second excited singlet state resulting from the large energy spacing (ΔE) between S_1 and S_2. The large energy gap leads to small Franck-Condon factors that slow internal conversion from S_2-S_1, making it possible for S_2-S_0 fluorescence to outcompete this radiationless process. This anomalous fluorescence emission agrees with that reported in the literature[2,32,50].

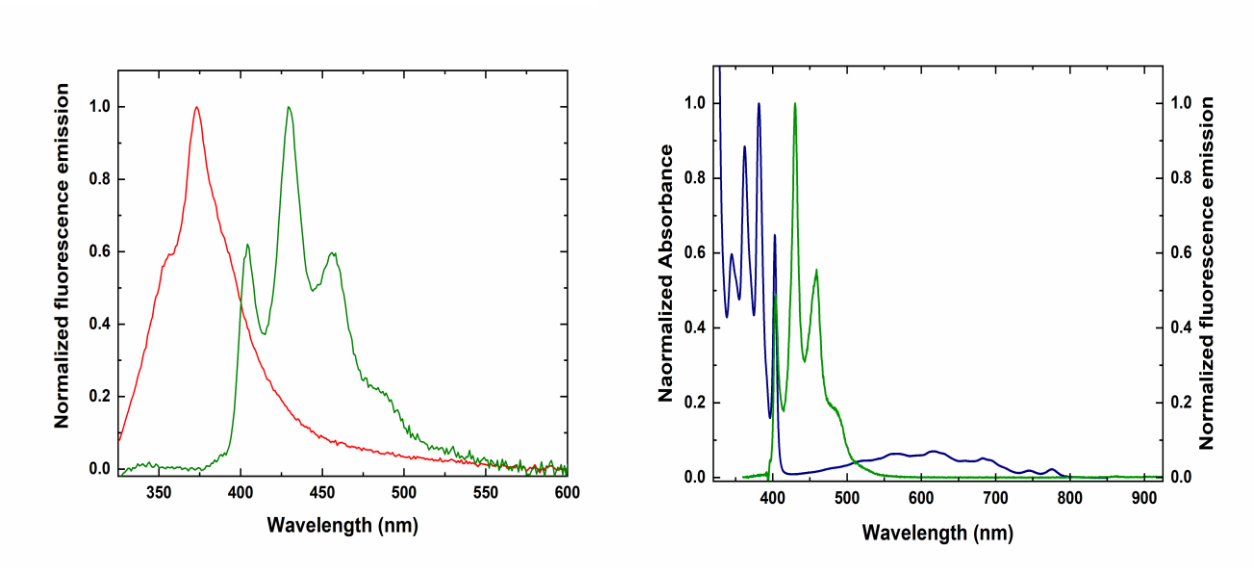

Figure 3.10: Normalized fluorescence emissions spectra of 10 µM 1,2-benzazulene (green) and azulene (red) in toluene for comparison at 320 nm excitation wavelength (left). The plot on the right displays the mirror image relationship between the normalized absorption (navy blue) and fluorescence (green) spectra excited at 355 nm for 50 µM 1,2-benzazulene. The background was corrected. The figure on the left is reproduced from reference[74]

The fluorescence spectra of 1,2-benzazulene, within 400 to 475 nm wavelength range (obtained by higher energy excitation), present a mirror image relationship between the absorption and fluorescence band at the S_2 (S_2-S_0) as illustrated in figure 3.10, right. The $S_2 \rightarrow S_0$ origin band for 1,2-benzazulene in toluene is centred at 24784 cm^{-1}. The ground state vibrational spacings are equal and follow a regular pattern, in agreement with the work done by *Binsch and coworkers*[34]. Also, the ground state vibrational spacing between the v" =1 and v"= 0 peaks in the emission spectrum yields a ground state fundamental frequency of 1450 cm^{-1}, which is slightly larger than the fundamental frequency estimated for its S_2 counterpart (azulene), as expected. This vibration is due to symmetric in-plane ring stretching obtained from the ground state Raman spectrum of 1,2-benzazulene (see Appendix 2A and 2B).

Several works on azulene spectroscopy suggest that excitation of azulene molecules in its $S_2 – S_0$ absorption bands show very weak $S_2 – S_1$ fluorescence emission[67]. In azulene, the $S_1 – S_0$ emission cannot be observed by mere excitation into its S_1 state. Previous reports on azulene[3] reveal that its $S_1 – S_0$ emission can only be noticed by thermally activated intersystem crossing to the first excited triplet state (T_1), which can be achieved by sensitization. However, unlike azulene, excitation of 1,2-benzazulene into its $S_2 – S_0$ absorption band shows a weak peak at $\lambda > 800$ nm. This weak peak is assignable to second order grating diffraction of the $S_2 – S_0$ fluorescence emission centred at 430 nm. The weak peak near the IR region ($\lambda > 800$ nm) was expected to be for the $S_2 – S_1$ and $S_1 – S_0$ emission regions. However, no measurable $S_2 – S_1$ and $S_1 – S_0$ fluorescence emissions were recorded even after excitation of 1,2-benzazulene into its weaker $S_1 – S_0$ absorption system. The $S_1 \rightarrow S_0$ fluorescence quantum yield and the S_1 lifetime for azulene have been studied and documented immensely in the literature using advanced techniques[16,79–81]. In reference to these research works, one can suggest that, for 1,2-benzazulene, the quantum yields that can be obtained from $S_2 – S_1$ and $S_1 – S_0$ fluorescence by direct excitation into these states can be estimated to be less than 3×10^{-7} on the basis of the similarity between the S_1-S_0 absorption spectra of azulene and 1,2-benzazulene.

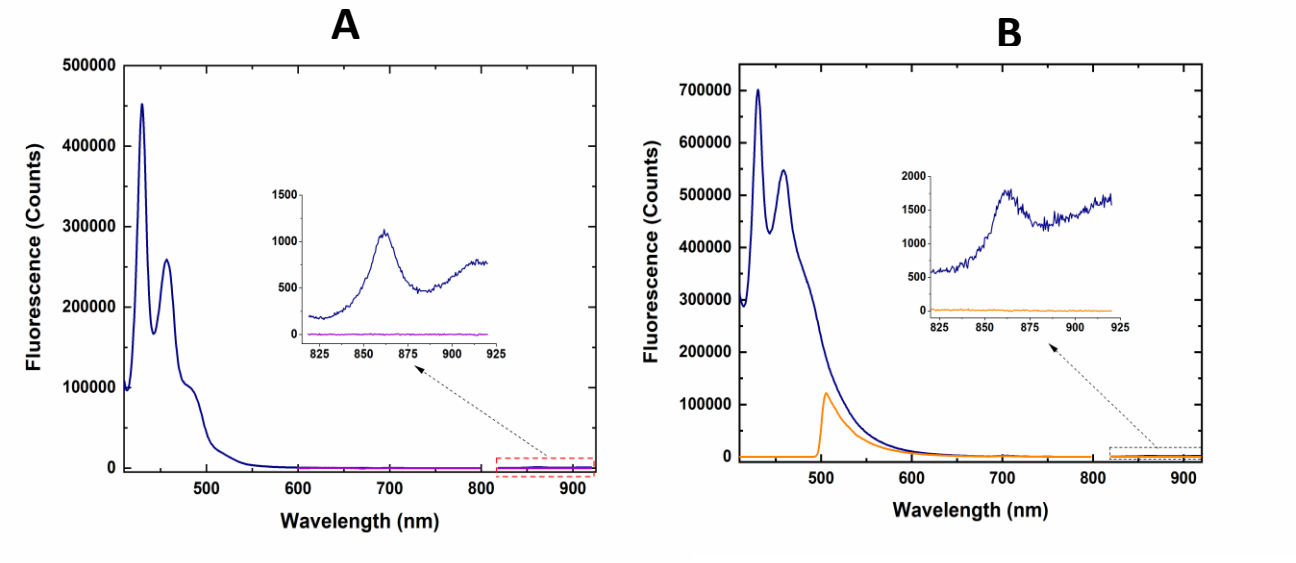

Figure 3.11: **A**: Fluorescence emission spectra of the 1,2-benzazulene in MCH at 405 nm and 561 nm excitation wavelength. The insert displays the second order grating diffraction of $S_2 - S_0$ fluorescence (navy blue) and the absence of $S_2 - S_1$ and $S_1 - S_0$ fluorescence even at 561 nm excitation (violet) at $\lambda > 800$ nm. **B:** Spectra showing a comparison of the second-order diffraction of the $S_2 - S_0$ fluorescence in the $\lambda > 800$ nm range in the presence (orange) and absence (navy blue) of 500 nm long-pass filter inserted into the emission path. Measurements were taken under the same condition. Spectra background corrected. Figure reproduced from the SI of reference[74]

3.2.2 Photophysics

To understand the photophysics of 1,2-benzazulene, we subjected it to time-resolved measurements, including non-linear fluorescence upconversion techniques at an excitation wavelength of 400 nm. The S_2 fluorescence decay times were determined for different concentrations in three solvents (MCH, MeOH and Tol). The fluorescence decay profiles were fitted with a single exponential decay function, as illustrated in figure 3.12.

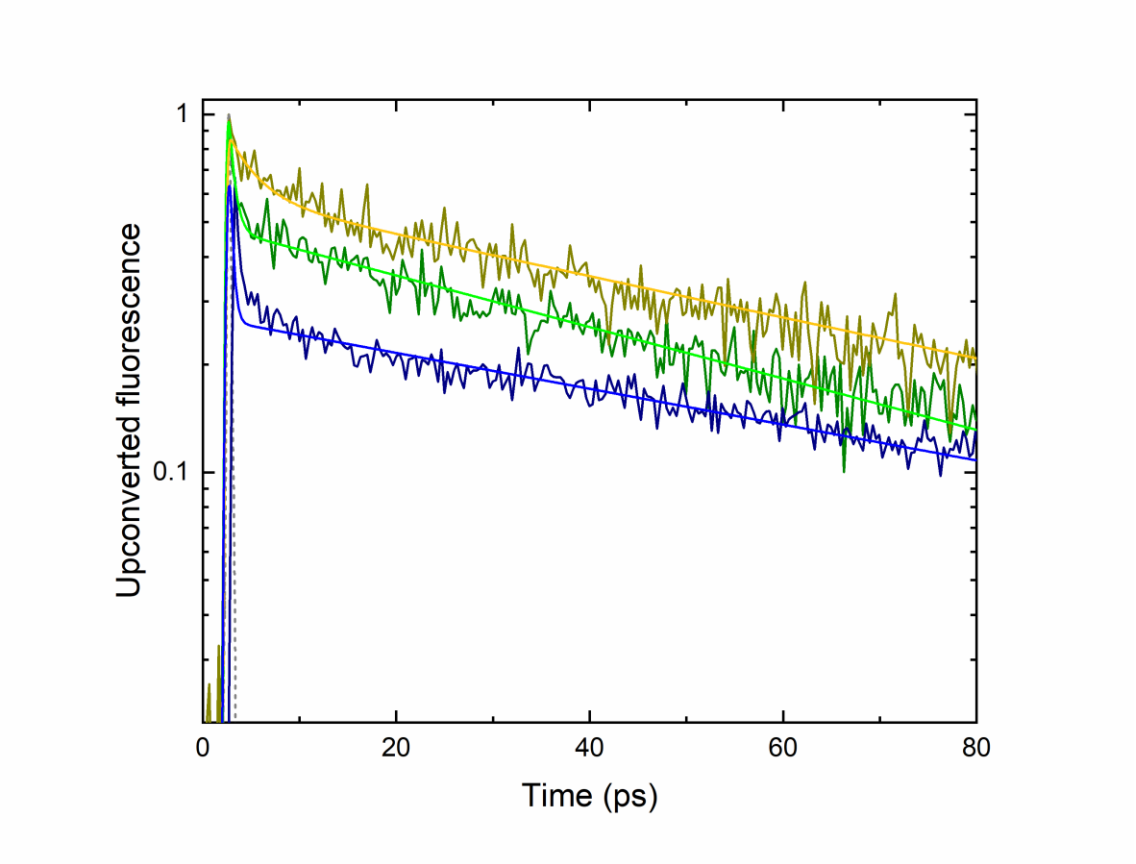

Figure 3.12: Upconverted S_2 fluorescence lifetime of 50 µM 1,2-benzazulene in methanol (dark yellow), methylcyclohexane (navy blue) and toluene (olive green) monitored at 435 nm. The solid lines indicate the fit to the instrument response function with single exponential fluorescence decay functions. The broken line shows the instrument response function curve determined at 462 nm. Figure reproduced from reference[74]

In order to accurately assign the S_2 lifetime of 1,2-benzazulene, a picosecond transient absorption experiment was carried out on 0.46 mM 1,2-benzazulene sample in THF by our collaborators at the University of Melbourne, Australia. The S_2 lifetime obtained from this measurement was 65 ps at 400 nm excitation wavelength after fitting the broad transient at various wavelengths within the 480 nm to 750 nm region (see Appendix 3). This measured lifetime (65 ps) is very similar to that obtained from the non-linear upconversion measurements in similar polar solvents.

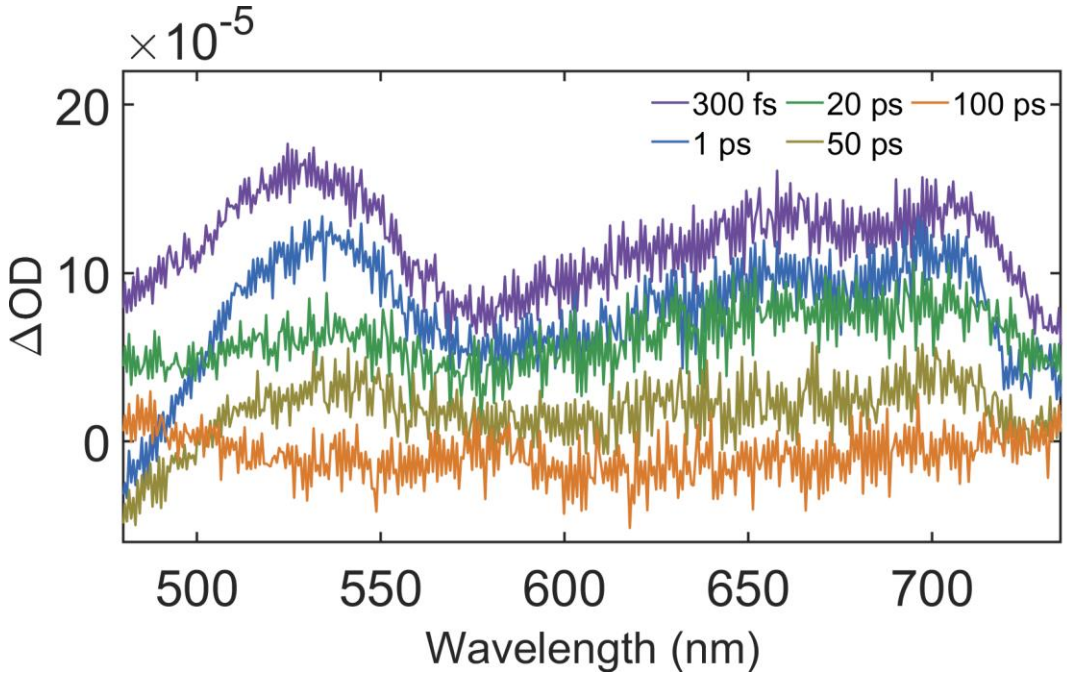

Figure 3.13: Picosecond transient absorption spectra of 0.46 mM 1,2-benzazulene in THF at an excitation wavelength of 400 nm as a function of pump-probe delay time measured by our collaborators in Australia. Figure reproduced from reference[74]

The major features of these transient absorption spectra agree with that obtained by *Muller, et al.*,[52] for 1,2-benzazulene in acetonitrile excited at 400 nm using a transient grating technique. Due to this similarity, one can also assign the lifetimes of the transients obtained from our experimental measurements to the S_2 of 1,2-benzazulene as reported by *Muller, et al.*[52]. This is because 1,2-benzazulene also exhibits S_2-S_0 fluorescence emission like azulene but with significantly weaker quantum yield[34,51].

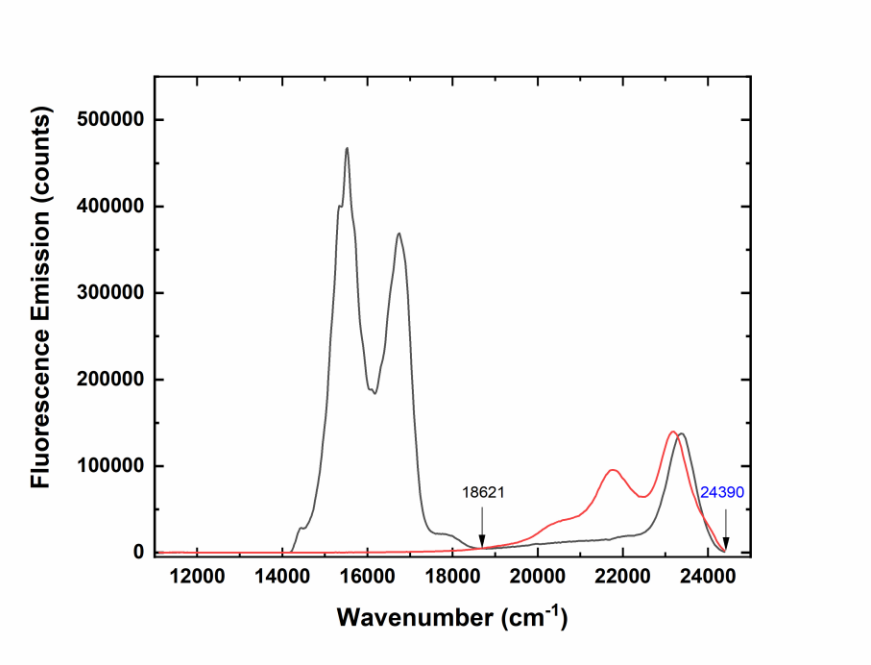

Figure 3.14: The fluorescence spectra used to determine the $S_2 - S_0$ fluorescence quantum yield of 32.67 µM 1,2-benzazulene(red) using 2.0 µM ZnTPP (black) as the reference standard, all in toluene. The samples have equal absorbances at the excitation wavelength, 405 nm. A customized SPEX spectrofluorometer was used in this measurement. The arrows indicate the region of integration to determine the $S_2 - S_0$ quantum yield. The experimental conditions for both measurements are the same. Figure reproduced from the SI of reference[74]

In this work, the S_2 quantum yield (ϕ_f) of 1,2-benzazulene was determined to calculate the radiative (Γ) and non-radiative (k_{nr}) decay rates from the S_2 state. The quantum yield of 1,2-benzazulene in toluene from the S_2 state was determined by excitation into its origin band using a 405 nm laser with ZnTPP in toluene as reference. From figure 3.14, the quantum yield was estimated to be 0.0020 ± 0.0001 with a measured lifetime of 66 ps. The calculations below show how the radiative and non-radiative decay rates were determined.

From eqn 1.2

$$\phi_F = \frac{\Gamma}{\Gamma + \sum k_{nr}} \qquad \text{eqn (1.2)}$$

$$0.002 = \frac{\Gamma}{\Gamma + \sum k_{nr}} \qquad \text{eqn (1.2a)}$$

From eqn 1.3

$$66 \text{ x } 10^{-12} \text{ s} = \frac{1}{\Gamma + \Sigma k_{nr}} \qquad \text{eqn (1.3a)}$$

Solving eqn (1.2a) and eqn (1.3a) simultaneously by substitution method yields

$$\Gamma = 3.0 \text{ x } 10^{7}\ s^{-1}$$

$$\Sigma k_{nr} = 1.5 \text{ x } 10^{10}\ s^{-1}$$

From the quantum yield and the S_2 lifetime values, the calculated radiative (Γ_{S2}) and sum of non-radiative (Σk_{nrS2}) decay rates were 3.0 x 10^7 s^{-1} and 1.5 x 10^{10} s^{-1} respectively in toluene as shown above. The table below shows the values obtained for the lifetime of 1,2-benzazulene and its radiative and non-radiative decay constants in different solvents. The decay data were obtained from fluorescence upconversion and transient absorption measurements.

Table 4: Kinetic parameters describing the radiative and non-radiative relaxation process of the excited electronic state of 1,2-benzazulene in several solvents obtained at room temperature.

1,2-benzazulene	solvent	τ (ps)	ϕ_f	Γ (s^{-1})	Σk_{nr} (s^{-1})
S_2	MCH	95 ± 5*			$1.0x10^{10}$
	toluene	66 ± 2	$2.3x10^{-3}$	$3.0x10^{7}$	$1.5x10^{10}$
	methanol	68 ± 3			$1.5x10^{10}$
	acetonitrile**	74			$1.4x10^{10}$
S_1	MCH	-	$<3x10^{-7}$		
	toluene	-	$<3x10^{-7}$	$2.0x10^{6}$	$>8x10^{12}$

* average of 6 trials, extrapolated to infinitely dilute solution.
** obtained from references 74 and 52.

Azulene and its fluorinated derivatives[71,82] are known to predominantly undergo S_2–S_1 radiationless decay from the S_2 state based on the energy gap law[19]. The value obtained for the Σk_{nrS2} at its measured $\Delta E(S_2 - S_1)$ reveal a significant energy gap correlation following the same trend as azulene and its fluorinated derivatives[71,82] as shown in figure 3.15. Based on this significant energy gap correlation, one can conclude that, like azulene and its fluorinated derivatives, the main decay path for 1,2-benzazulene from the S_2 state is internal conversion to the S_1 state.

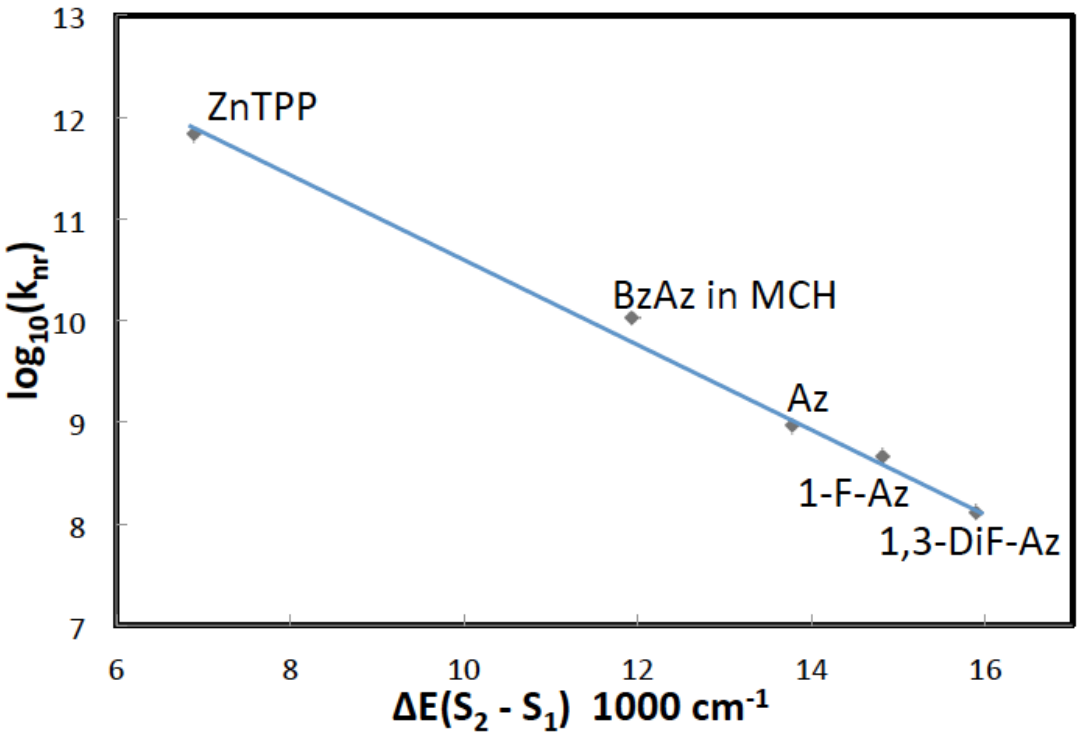

Figure 3.15: Energy gap correlation of the non-radiative decay rate of the S_2 state of 1,2-benzazulene with azulene, 1-fluoroazulene, 1,3-difluoroazulene and ZnTPP in toluene, demonstrating that their main decay path from the S_2 state is internal conversion to the S_1. The data for 1,2-benzazulene can be found in tables 3 and 4. Figure reproduced from reference[74]

Like azulene, 1,2-benzazulene shows no visible $S_1 - S_0$ fluorescence emission after either internal conversion from S_2 to S_1 or direct excitation to higher vibrational levels of S_1 (see figure 3.10). This suggests that similar to azulene, the S_1 state of 1,2-benzazulene undergoes rapid internal conversion to high vibrational levels of its S_0 state, rendering fluorescence emission from the S_1 state improbable. From our experimental measurements on 1,2-benzazulene, the radiative decay rate from the S_1 state(k_{rS1}) was calculated to be 2.0 x 10^6 s^{-1} using the oscillator strength ratio of the absorption spectra, $f_{S2\text{-}S0}/f_{S1\text{-}S0}$ and the value of the radiative decay rate from the S_2 as indicated on the calculation below.

$$\frac{f_{S2-S0}}{f_{S1-S0}} \approx \frac{\Gamma_{S2}}{\Gamma_{S1}}$$

$$\Gamma_{S1} \approx \frac{f_{S1-S0}}{f_{S2-S0}} \text{ x } \Gamma_{S2}$$

$$\Gamma_{S1} \approx \frac{1}{13} \text{ x } 3.0 \text{ x } 10^{7}\ s^{-1} \approx 2.3 \text{ x } 10^{6}\ s^{-1}$$

The S_1 quantum yield (ϕ_{fS1}) was not determined in this work as there is no evidence of measurable $S_0 \rightarrow S_1$ fluorescence emission due to instrumental limitations. However, previous report in the literature[81] suggests that the estimated quantum yield for $S_1 - S_0$ fluorescence (ϕ_{fS1}) < 3 x 10^{-7}. Based on the values of the ϕ_{fS1} and the $k_{rS1,}$ the non-radiative decay rate constant of vibrationally hot S_1 state (k_{nrS1}) can be projected to be greater than 8 x 10^{12} s^{-1}. This value clearly suggests that radiationless decay from S_1-S_0 is very rapid compared to intermolecular vibrational relaxation rates in solution (an example is energy transfer to solvent molecules). From this, one can conclude that like azulene, 1,2-benzazulene undergoes ultrafast internal conversion from the S_1 to the S_0 state resulting from the conical intersection of their respective potential energy surfaces, making it possible for radiationless decay to occur rapidly at the expense of fluorescence emission.

Having understood the spectroscopy and the photophysics of dilute solutions of 1,2-benzazulene, it is advantageous to subject this molecule to aggregation studies to explore its spectroscopic and photophysical properties at higher concentrations. Spectroscopic studies on 1,2-benzazulene at high concentration, *ca* 0.01 M in MCH (near solute saturation), reveal no evidence of ground state aggregation. Non-linear fluorescence upconversion measurement on the various concentrations of 1,2-benzazulene reveals a marginal decrease in S_2 lifetimes as concentration increases towards the saturation range. The decrease in the S_2 lifetimes, even though statistically weak, suggests self-quenching in 1,2-benzazulene. This process occurs at a rate no greater than the diffusion-controlled limit compared to azulene, whose quenching mechanism from the S_2 state is partly by a diffusion-controlled process with a diffusion rate constant of 1.5 x 10^{10} $M^{-1}s^{-1}$ and a

static quenching component. In addition, Förster resonance energy transfer (FRET) occurring via $S_2 + S_0 \rightarrow 2S_1$ in 1,2-benzazulene is eliminated. The magnitude of energy transfer is also determined by the extent of spectral overlap between the emission and absorption spectra. Like azulene, the overlap between the $S_2 \rightarrow S_0$ fluorescence and $S_0 \rightarrow S_1$ absorption spectra that permit Förster resonance energy transfer (FRET) in 1,2-benzazulene is insignificant. This is evident from the weak $S_0 - S_1$ absorption spectrum as shown in figure 3.9 and the very small $S_2 - S_1$ fluorescence quantum yield. However, subjecting pure 1,2-benzazulene solid thin-film to absorption measurement shows obvious evidence of aggregation, as indicated in figure 3.8B. The formation of the benzazulene aggregates results from the interaction of 1,2-benzazulene molecules due to π-π stacking. The net effect of this interaction is the extension of the pi-conjugation system and stronger exciton coupling in the 1,2-benzazulene aggregates. This is clearly visible from the absorption spectrum in figure 3.8B, where the absorption spectrum is broad and shifted to a longer wavelength than the monomer. It is previously documented[83] that the π-π interaction between the azulene molecules involves a significant overlap between the electron-rich five-membered ring of one azulene moiety and the electron-deficient seven-membered ring of another azulene unit at specific orientation and π-π distance[84]. The annelation of benzene to the 1,2-position increases the nucleophilicity of the five-membered ring. This enhances the π-π interaction of the 1,2-benzazulene molecules. Steady-state fluorescence measurement on the 1,2-benzazulene thin film shows no measurable S_2-S_0 fluorescence emission at excitation wavelength selected close to and towards the red of the $S_0 - S_2$ absorption spectrum of the monomer.

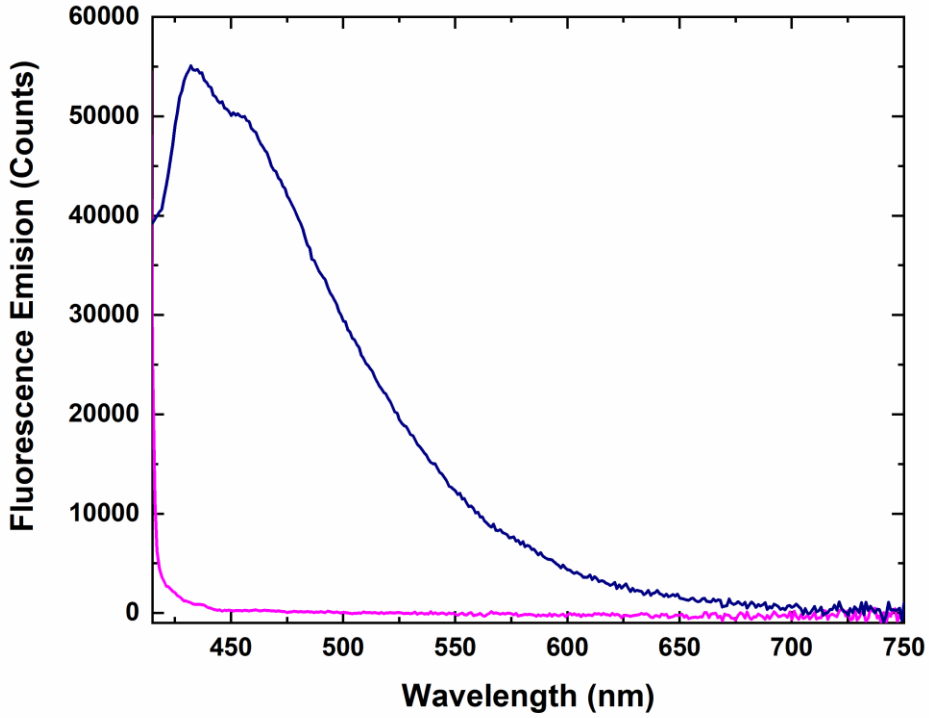

Figure 3.16: Comparison of fluorescence spectra of 50 µM 1,2 benzazulene solution in MCH and two layers of 1,2-benzazulene thin film dropcasted onto a quartz disc. The spectra display no observable S_2 fluorescence emission from the thin film (magenta) and evidence of S_2 fluorescence emission for the monomer. All experimental conditions are the same.

The result obtained from this work is consistent with the study done by *Ferguson, et al.*[39], where there is no evidence of S_2 fluorescence observed from the steady-state fluorescence measurement of ground state azulene dimers. These experimental findings and similar research in the literature[3,19,39] question the mechanism of fluorescence quenching in azulene aggregates and its dimers. It can, however, be proposed that, the close proximity of 1,2-benzazulene molecules due to π-π interaction in the aggregate formation accounts to a large extent for the S_2 fluorescence quenching process. The absence of the S_2 fluorescence, as observed from figure 3.16, suggests an ultrafast radiationless decay process within the picoseconds range in the amorphous solid which possibly may include singlet fission. However, the mechanism of the SF process via $S_2 + S_0 \rightarrow T_1 + T_1$ in these solid thin-films cannot be clearly established at this point since there is no evidence

of triplet formation under S_2 excitation. Therefore, the need for further studies into how the crystallinity of the solid thin film influences S_2 fluorescence quenching in 1,2-benzazulene and investigation of singlet fission process and its mechanism in these solid thin films.

Chapter 4: Conclusion

This section concludes by highlighting the significant similarities and differences in the spectroscopy and photophysics of 1,2-benzazulene and azulene. The result obtained from this experiment suggests that the S_1-S_0 absorption bands that correspond to azulene are also present in 1,2-benzazulene. In 1,2-benzazulene, the S_1-S_0 absorption bands are shifted to a longer wavelength than azulene due to the benzene ring annelation. These bands look similar in shape and are relatively weak in intensity compared to the S_2-S_0 absorption band. The similarity in the S_1-S_0 absorption bands between these two molecules shows that the fusion of the benzene ring to the azulene ring does not significantly affect the structure of the first absorption band of 1,2-benzazulene compared to azulene. However, the S_2-S_0 absorption spectrum for 1,2-benzazulene looks different from that of azulene. In 1,2-benzazulene, the S_2-S_0 absorption spectrum exhibits distinct vibrational structures with a strong S_2-S_0 origin band with approximately equal vibrational spacing from v' = 0 to v' = 3 (Franck-Condon series) resulting from the fusion of the benzene ring to azulene. Like azulene, 1,2-benzazulene also emits anomalous fluorescence from the S_2 State due to the large energy gap between the S_2 and S_1. However, unlike azulene, the S_0-S_2 absorption and fluorescence spectra show an obvious mirror image relationship indicating the same transitions are most favourable for absorption and emission at the S_2 state. No S_2–S_1 and S_1–S_0 fluorescence emissions are observed for both azulene and 1,2-benzazulene, suggesting that similar to azulene, 1,2-benzazulene also undergo rapid S_1-S_0 internal conversion bypassing T_1. This results from the conical intersection of the S_1 and S_0 potential energy surfaces, making it possible for radiationless decay via this route to be more probable than fluorescence emission. However, excitation of 1,2-benzazulene into its S_2 – S_0 absorption band shows a weak peak at $\lambda > 800$ nm assignable to second order grating diffraction of the S_2 – S_0 fluorescence emission centred at 430 nm. Aggregation studies on azulene using steady-state fluorescence measurements reveal a decrease in S_2

fluorescence intensity as concentration increases. This is due to fluorescence self-quenching from the S_2 state. To understand the quenching mechanism and the photophysics of azulene and 1,2-benzazulene, these two molecules have been subjected to time-resolved measurements. TCSPC measurement on various concentrations of azulene displays a decrease in the S_2 fluorescence lifetime as the concentration increases, similar to the S_2 fluorescence intensity decrease as noticed in the fluorescence spectra of azulene. Stern-Volmer plot using the ratio of S_2 fluorescence lifetime and fluorescence intensity as a function of concentration shows that the quenching mechanism of azulene from the S_2 is diffusion-controlled with a static quenching component. The time-dependent diffusion rate constant (k_q) obtained from this measurement was 1.5×10^{10} $M^{-1}s^{-1}$, similar to that reported by *Reis e Sousa, et al.*[1]. On this basis, we conclude that the quenching mechanism of azulene from the S_2 state partly includes a short-range non-radiative energy transfer from $S_2 \rightarrow S_1$ and $S_1 \rightarrow S_0$ radiationless processes. For 1,2-benzazulene, other time-resolved techniques are used to investigate its photophysical properties due to its shorter S_2 fluorescence lifetime. Picosecond transient absorption measurement conducted on the solution phase samples of 1,2-benzazulene shows a broad absorption spectrum assigned to the S_2 state but shows no evidence of triplet formation(T_1). The S_2 lifetime obtained from the transient absorption measurement was 65ps, similar to the lifetimes obtained for the non-linear fluorescence upconversion measurements in similar polar solvents. The calculated non-radiative decay rate constant from the S_2 (k_{nrS2}) of 1,2-benzazulene at its measured $\Delta E(S_2 - S_1)$ reveals an energy gap correlation following the same trend as azulene and its fluorinated derivatives. One can now conclude that like azulene and its fluoroderivatives, S_2-S_1 internal conversion is the main decay path for 1,2-benzazulene. Also, steady-state absorption, fluorescence and time-resolved measurement conducted on the solution phase of 1,2-benzazulene at high concentrations (approximately 0.01 M in MCH) showed no obvious evidence of fluorescence self-quenching from the S_2 state compared to azulene, where

fluorescence self-quenching from the S_2 is evident at a similar concentration range. The recent work done by *Wenjun and coworkers* on singlet fission from upper excited electronic states of cofacial perylene dimers brings to light the possibility of singlet fission from the second excited singlet state[53]. There are also hints in the literature suggesting that singlet fission may occur in azulene aggregates [3,39,45,54] or some of its derivatives via $S_2 + S_0 \rightarrow 2T_1$[3]. We approach this work with a similar focus. However, the electronic spectra of 1,2-benzazulene obtained from our experimental measurements suggest that such a singlet fission process via $S_2 + S_0 \rightarrow 2T_1$ would be near thermoneutral. But then, absorption spectrum obtained from the solid thin film of 1,2-benzazulene shows the formation of aggregates with no measurable S_2 fluorescence and no evidence of transient absorption signal assignable to T_1. Based on this occurrence, one can conclude that the radiationless decay from the S_2 in 1,2-benzazulene thin films must be ultrafast. However, the mechanism of this ultrafast decay process can not be fully established at this point but is yet to be explored.

4.1: Future work

In subsequent studies, the mechanism for the ultrafast S_2 decay in 1,2-benzazulene thin-films will be investigated further. There are possibilities that this ultrafast S_2 decay may include singlet fission process. In order to understand the mechanism of this rapid decay process, it is important to ensure the homogeneity of the film, hence requires further studies on how this can be achieved. For instance, using spin-coating techniques and adding polymer binders such as Poly(methyl methacrylate) during film preparation are known to enhance the homogeneity of thin-films. Also, it will be important to study the crystallinity of the thin-films using x-ray diffraction techniques to investigate the packing of the 1,2-benzazulene molecules and how they are perhaps conducive for singlet fission process. Solvent-vapor and thermal annealing have been reported to

dramatically alter the crystallinity and the singlet exciton fission dynamics of thin films[85,86]. As such, it will be advantageous to treat 1,2-benzazulene solid thin-films with a similar focus.

Chapter 5: References

(1) Reis e Sousa, A. T.; Martinho, J. M. G.; Baros, F.; André, J. C. Self-Quenching of Azulene Fluorescence in Cyclohexane. *J. Photochem. Photobiol. A Chem.* **1994**, *83* (3), 199–203. https://doi.org/10.1016/1010-6030(94)03834-1.

(2) Beer, M.; Longuet-Higgins, H.C. Anomalous Light Emission of Azulene. *J. Chem. Phys.* **1955**, *23* (8), 1390–1391. https://doi.org/10.1063/1.1742314.

(3) Nickel, B.; Klemp, D. The Lowest Triplet State of Azulene-h_8 and Azulene-d_8 in Liquid Solution. I. Survey, Kinetic Considerations, Experimental Technique, and Temperature Dependence of Triplet Decay. *Chem. Phys.* **1993**, *174* (2), 297–318. https://doi.org/10.1016/0301-0104(93)87014-E.

(4) Jain, A.; Blum, C.; Subramaniam, V. Fluorescence Lifetime Spectroscopy and Imaging of Visible Fluorescent Proteins, First Edit.; *Elsevier*, **2009**. https://doi.org/10.1016/B978-0-444-53075-2.00004-6.

(5) Etinski, M.; Tatchen, J.; Marian, C. M. Time-Dependent Approaches for the Calculation of Intersystem Crossing Rates. *J. Chem. Phys.* **2011**, *134* (15), 0–9. https://doi.org/10.1063/1.3575582.

(6) Jaffé, H. H.; Miller, A. L. The Fates of Electronic Excitation Energy. *J. Chem. Educ.* **1966**, *43* (9), 469–473. https://doi.org/10.1021/ed043p469.

(7) Ellis, A. M.; Feher, M.; Wright, T. G. Electronic and Photoelectron Spectroscopy: Fundamentals and Case Studies. *Electron. Photoelectron Spectrosc. Fundam. Case Stud.* **2005**, *9780521817* (June), 1–286. https://doi.org/10.1017/CBO9781139165037.

(8) Omary, M. A.; Patterson, H. H. Luminescence, Theory, 3rd ed.; *Elsevier Ltd.*, **2016**. https://doi.org/10.1016/B978-0-12-803224-4.00193-X.

(9) Uzer, T.; Miller, W. H. Theories of Intramolecular Vibrational Energy Transfer. *Phys. Rep.* **1991**, *199* (2), 73–146. https://doi.org/10.1016/0370-1573(91)90140-H.

(10) Kogure, T.; Kawano, H.; Abe, Y.; Miyawaki, A. Fluorescence Imaging Using a Fluorescent Protein with a Large Stokes Shift. *Methods* **2008**, *45* (3), 223–226. https://doi.org/10.1016/j.ymeth.2008.06.009.

(11) Coolidge, A. S.; James, H. M.; Present, R. D. A Study of the Franck-Condon Principle. *J. Chem. Phys.* **1936**, *4* (3), 193–211. https://doi.org/10.1063/1.1749818.

(12) Liu, R. S. H.; Asato, A. E. Tuning the Color and Excited State Properties of the Azulenic Chromophore: NIR Absorbing Pigments and Materials. *J. Photochem. Photobiol. C Photochem. Rev.* **2003**, *4* (3), 179–194. https://doi.org/10.1016/j.jphotochemrev.2003.09.001.

(13) Itoh, T. Fluorescence and Phosphorescence from Higher Excited States of Organic Molecules. *Chem. Rev.* **2012**, *112* (8), 4541–4568. https://doi.org/10.1021/cr200166m.

(14) Xin, H.; Gao, X. Application of Azulene in Constructing Organic Optoelectronic Materials: New Tricks for an Old Dog. *Chempluschem* **2017**, *82* (7), 945–956. https://doi.org/10.1002/cplu.201700039.

(15) Liu, R. S. H.; Muthyala, R. S.; Wang, X. S.; Asato, A. E.; Wang, P.; Ye, C. Correlation of Substituent Effects and Energy Levels of the Two Lowest Excited States of the Azulenic Chromophore. *Org. Lett.* **2000**, *2* (3), 269–271. https://doi.org/10.1021/ol990324w.

(16) Huppert, D.; Jortner, J.; Rentzepis, P. M. $S_2 \rightarrow S_1$ Emission of Azulene in Solution. *Chem. Phys. Lett.* **1972**, *13* (3), 225–228. https://doi.org/10.1016/0009-2614(72)85047-4.

(17) Tittelbach-Helmrich, D.; Wagner, B. D.; Steer, R. P. Subpicosecond Vibrational Relaxation of the S_1 States of Azulene and Guaiazulene in Solution. *Can. J. Chem.* **1995**, *73* (2), 303–306. https://doi.org/10.1139/v95-041.

(18) Michl, J.; Thulstrup, E. W. Why Is Azulene Blue and Anthracene White? A Simple Mo Picture. *Tetrahedron* **1976**, *32* (2), 205–209. https://doi.org/10.1016/0040-4020(76)87002

(19) Steer, R. P. Photophysics of Molecules Containing Multiples of the Azulene Carbon Framework. *J. Photochem. Photobiol. C Photochem. Rev.* **2019**, *40*, 68–80. https://doi.org/10.1016/j.jphotochemrev.2019.06.002.

(20) Shevyakov, S. V.; Li, H.; Muthyala, R.; Asato, A. E.; Croney, J. C.; Jameson, D. M.; Liu, R. S. H. Orbital Control of the Color and Excited State Properties of Formylated and Fluorinated Derivatives of Azulene. *J. Phys. Chem. A* **2003**, *107* (18), 3295–3299. https://doi.org/10.1021/jp021605f.

(21) Gudmundsdóttir, A. D. Organic Photochemistry and Photophysics. Molecular and Supramolecular Photochemistry, Volume 14 Edited by Vaidhyanathan Ramamurthy (University of Miami) and Kirk S. Schanze (University of Florida). CRC Press/Taylor & F Vol. 128. https://doi.org/10.1021/ja069719i.

(22) Xin, H.; Ge, C.; Jiao, X.; Yang, X.; Rundel, K.; McNeill, C. R.; Gao, X. Incorporation of 2,6-Connected Azulene Units into the Backbone of Conjugated Polymers: Towards High-Performance Organic Optoelectronic Materials. *Angew. Chemie - Int. Ed.* **2018**, *57* (5), 1322–1326. https://doi.org/10.1002/anie.201711802.

(23) Wang, X.; Ng, J. K. P.; Jia, P.; Lin, T.; Cho, C. M.; Xu, J.; Lu, X.; He, C. Synthesis, Electronic, and Emission Spectroscopy, and Electrochromic Characterization of Azulene-Fluorene Conjugated Oligomers and Polymers. *Macromolecules* **2009**, *42* (15), 5534–5544. https://doi.org/10.1021/ma900847r.

(24) Englman, R. The Energy Gap Law for Radiationless Transitions in Large Molecules. *Mol. Phys.* **1969**, *18* (May 1970), 145–164.

(25) Ito, S.; Inabe, H.; Okujima, T.; Morita, N.; Watanabe, M.; Harada, N.; Imafuku, K. Synthesis and Redox Behavior of Azulene-Substituted Benzene Derivatives and H5-Cyclopentadienyl)[Tetra- and Di(6-Azulenyl) Cyclobutadiene]Cobalt Complexes. *J. Org. Chem.* **2001**, *66* (21), 7090–7101. https://doi.org/10.1021/jo010540u.

(26) Platt, J. R. Classification of Spectra of Cata-Condensed Hydrocarbons. *J. Chem. Phys.* **1949**, *17* (5), 484–495. https://doi.org/10.1063/1.1747293.

(27) Higashi, M.; Yamaguchi, H.; Schmidt, W. Photoelectron Spectra of Benzazulenes. *J. Chem. Soc. Faraday Trans. 2 Mol. Chem. Phys.* **1987**, *83* (5), 741–745. https://doi.org/10.1039/F29878300741.

(28) Xin, H.; Gao, X. Application of Azulene in Constructing Organic Optoelectronic

Materials: New Tricks for an Old Dog. *Chempluschem* **2017**, *82* (7), 945–956. https://doi.org/10.1002/cplu.201700039.

(29) Das Gupta, A.; Chatterjee, S.; Das Gupta, N. K. Theoretical Studies of Some Nonbenzenoid Hydrocarbons. V. Benzazulenes and Benzofluoranthenes. *Bull. Chem. Soc. Jpn.* **1979**, *52* (10), 3070–3075. https://doi.org/10.1246/bcsj.52.3070.

(30) Conrow, K. Org. *Synthesis (Stuttg).* **1963**, 101–104.

(31) Sperandio, D.; Hansen, H. -J. An Efficient Straightforward Synthesis of Benz[a]Azulene. *Helv. Chim. Acta* **1995**, *78* (3), 765–771. https://doi.org/10.1002/hlca.19950780321.

(32) Otteson, D.; Michl, J.; Jutz, C. Magnetic Circular Dichroism of Cyclic π -Electron Systems. 151. Benzazulenes. *J. Am. Chem. Soc.* **1978**, *100* (22), 6882–6883. https://doi.org/10.1021/ja00490a015.

(33) Heilbronner, E.; Murrell, J. N. A Theoretical Study of the Electronic Spectra of the Benzazulenes and Benzologue-Tropylium Cations and a Critical Examination of the Perimeter Model. *Mol. Phys.* **1963**, *6* (1), 1–18. https://doi.org/10.1080/00268976300100011.

(34) Binsch, G.; Heilbronner, E.; Jankow, R.; Schmidt, D. On the Fluorescence Anomaly of Azulene. *Chem. Phys. Lett.* **1967**, *1* (4), 135–138. https://doi.org/10.1016/0009-2614(67)85008-5.

(35) Michl, J. Magnetic Circular Dichroism of Cyclic π-Electron Systems. 3.1 Classification of Cyclic π Chromophores with a (4N + 2)-Electron [n]Annulene Perimeter and General Rules for Substituent Effects on the MCD Spectra of Soft Chromophores. *J. Am. Chem. Soc.* **1978**, *100* (22), 6819–6824. https://doi.org/10.1021/ja00490a003.

(36) Zhang, X. H.; Li, C.; Wang, W. B.; Cheng, X. X.; Wang, X. S.; Zhang, B. W. Photophysical, Electrochemical, and Photoelectrochemical Properties of New Azulene-Based Dye Molecules. *J. Mater. Chem.* **2007**, *17* (7), 642–649. https://doi.org/10.1039/b613703b.

(37) Más-Montoya, M.; Janssen, R. A. J. The Effect of H- and J-Aggregation on the Photophysical and Photovoltaic Properties of Small Thiophene–Pyridine–DPP Molecules for Bulk-Heterojunction Solar Cells. *Adv. Funct. Mater.* **2017**, *27* (16). https://doi.org/10.1002/adfm.201605779.

(38) Kasha, M.; Rawls, H. R.; El-Bayoumi, M. A. The Exciton Model In Molecular Spectroscopy. *Pure Appl. Chem.* **1965**, *11* (3–4), 371–392. https://doi.org/10.1351/pac196511030371.

(39) Ferguson, J.; Mau, W.; Morris, J. M. Spectra of Azulene Dimers. *Aust. J. Chem.* **1974**, *27* (4), 713–719. https://doi.org/10.1071/CH9740713.

(40) Montero, M. T.; Hernández, J.; Estelrich, J. Fluorescence Quenching of Albumin. A Spectrofluorimetric Experiment. *Biochem. Educ.* **1990**, *18* (2), 99–101. https://doi.org/https://doi.org/10.1016/0307-4412(90)90188-T

(41) Rice, S.A. In Comprehensive Chemical Kinetics. Diffusssion-Limited Reaction. *Elsevier.* **1985**, vol. *25*. https://ci.nii.ac.jp/naid/10012700148/en/

(42) Lakowicz JR, editor. Principles of Fluorescence Spectroscopy. Springer US; 2006; Available from:http://dx.doi.org/10.1007/978-0-387-46312-4.

(43) Lee, J.; Jadhav, P.; Reusswig, P. D.; Yost, S. R.; Thompson, N. J.; Congreve, D. N.; Hontz, E.; Van Voorhis, T.; Baldo, M. A. Singlet Exciton Fission Photovoltaics. *Acc. Chem. Res.* **2013**, *46* (6), 1300–1311. https://doi.org/10.1021/ar300288e.

(44) Nandi, A.; Manna, B.; Ghosh, R. Singlet Fission Dynamics in the 5,12-Bis(Phenylethynyl)Tetracene Thin Film. *J. Phys. Chem. C* **2021**, *125* (4), 2583–2591. https://doi.org/10.1021/acs.jpcc.0c05382.

(45) Smith, M. B.; Michl, J. Singlet Fission. *Chem. Rev.* **2010**, *110* (11), 6891–6936. https://doi.org/10.1021/cr1002613.

(46) Casanova, D. Theoretical Modeling of Singlet Fission. *Chem. Rev.* **2018**, *118* (15), 7164–7207. https://doi.org/10.1021/acs.chemrev.7b00601.

(47) Fallon, K. J.; Budden, P.; Salvadori, E.; Ganose, A. M.; Savory, C. N.; Eyre, L.; Dowland, S.; Ai, Q.; Goodlett, S.; Risko, C.; Scanlon, D. O.; Kay, C. W. M.; Rao, A.; Friend, R. H.; Musser, A. J.; Bronstein, H. Exploiting Excited-State Aromaticity To Design Highly Stable Singlet Fission Materials. *J. Am. Chem. Soc.* **2019**, *141* (35), 13867–13876. https://doi.org/10.1021/jacs.9b06346.

(48) Paci, I.; Johnson, J. C.; Chen, X.; Rana, G.; Popović, D.; David, D. E.; Nozik, A. J.; Ratner, M. A.; Michl, J. Singlet Fission for Dye-Sensitized Solar Cells: Can a Suitable Sensitizer Be Found? *J. Am. Chem. Soc.* **2006**, *128* (51), 16546–16553. https://doi.org/10.1021/ja063980h.

(49) Wen, J.; Havlas, Z.; Michl, J. Captodatively Stabilized Biradicaloids as Chromophores for Singlet Fission. *J. Am. Chem. Soc.* **2015**, *137* (1), 165–172. https://doi.org/10.1021/ja5070476.

(50) Yamaguchi, H.; Sato, S.; Yasunam, M.; Sato, T.; Yoshinobu, M. Anomalous Fluorescence Spectra of Benz[a]Azulene Derivatives. *Spectrochim. Acta - Part A Mol. Biomol. Spectrosc.* **1997**, *53* (14), 2471–2473. https://doi.org/10.1016/S1386-1425(97)00151-0.

(51) Yamaguchi, H.; Ninomiya, K.; Fukuda, M.; Itô, S.; Kato, N.; Fukazawa, Y. Magnetic Circular Dichroism and Anomalous Fluorescence Spectra of [2,2] (2,6)Azulenophanes. *Chem. Phys. Lett.* **1980**, *72* (2), 297–300. https://doi.org/10.1016/0009-2614(80)80295-8.

(52) Muller, P. A.; Vauthey, E. Charge Recombination Dynamics of Geminate Ion Pairs Formed by Electron Transfer Quenching of Molecules in an Upper Excited State. *J. Phys. Chem. A* **2001**, *105* (25), 5994–6000. https://doi.org/10.1021/jp010015z.

(53) Ni, W.; Gurzadyan, G. G.; Zhao, J.; Che, Y.; Li, X.; Sun, L. Singlet Fission from Upper Excited Electronic States of Cofacial Perylene Dimer. *J. Phys. Chem. Lett.* **2019**, *10* (10), 2428–2433. https://doi.org/10.1021/acs.jpclett.9b00717.

(54) Phillips, D.; Christensen, R. L. Time Correlated Single-Photon Counting (TCSPC) Using Laser Excitation. *Instrum. Sci. Technol.* **1985**, *14* (3–4), 267–292. https://doi.org/10.1080/10739148508543581.

(55) O'Connor, D. V; Philips, D. Time-Correlated Single Photon Counting. Academic Press. **1984**. ISBN-10: 0125241402. https://doi.org/10.1351/goldbook.t06377.

(56) Tripathy, U.; Kowalska, D.; Liu, X.; Velate, S.; Steer, R. P. Photophysics of Soret-Excited Tetrapyrroles in Solution. I. Metalloporphyrins: MgTPP, ZnTPP, and CdTPP. *J. Phys. Chem. A* **2008**, *112* (26), 5824–5833. https://doi.org/10.1021/jp801395h.

(57) Schanz, R.; Kovalenko, S. A.; Kharlanov, V.; Ernsting, N. P. Broad-Band Fluorescence Upconversion for Femtosecond Spectroscopy. *Appl. Phys. Lett.* **2001**, *79* (5), 566–568. https://doi.org/10.1063/1.1387257.

(58) Chosrowjan, H.; Taniguchi, S.; Tanaka, F. Ultrafast Fluorescence Upconversion Technique and Its Applications to Proteins. *FEBS J.* **2015**, *282* (16), 3003–3015. https://doi.org/10.1111/febs.13180.

(59) Sundström, V.; Pullerits, T.; Van Grondelle, R. Photosynthetic Light-Harvesting: Reconciling Dynamics and Structure of Purple Bacterial LH2 Reveals Function of Photosynthetic Unit. *J. Phys. Chem. B* **1999**, *103* (13), 2327–2346. https://doi.org/10.1021/jp983722+.

(60) Van Amerongen, H.; Van Grondelle, R. Understanding the Energy Transfer Function of LHCII, the Major Light-Harvesting Complex of Green Plants. *J. Phys. Chem. B* **2001**, *105* (3), 604–617. https://doi.org/10.1021/jp0028406.

(61) Van Grondelle, R.; Dekker, J. P.; Gillbro, T.; Sundstrom, V. Energy Transfer and Trapping in Photosynthesis. *Biochim. Biophys. Acta - Bioenerg.* **1994**, *1187* (1), 1–65. https://doi.org/https://doi.org/10.1016/0005-2728(94)90166-X.

(62) Berera, R.; Van Grondelle, R.; Kennis, J. T. M. Ultrafast Transient Absorption Spectroscopy: Principles and Application to Photosynthetic Systems. *Photosynth. Res.* **2009**, *101* (2–3), 105–118. https://doi.org/10.1007/s11120-009-9454-y.

(63) Burdzinski, G.; Pino, T.; Changenet, P. Transient Absorption in Inorganic Systems. *Springer Handbook of Inorganic Chemistry*. **2020**, In press. Hal-02991509. https://hal.archives-ouvertes.fr/hal-02991509.

(64) Dragu, E. A.; Nica, S.; Raicopol, M.; Baran, A.; Anghel, D. F.; Cojocaru, B.; Tarko, L.; Razus, A. C. Synthesis, Solid-State Photophysical Properties and Electropolymerization of Novel Diazulenyl Ethenes. *Tetrahedron Lett.* **2012**, *53* (21), 2611–2614. https://doi.org/10.1016/j.tetlet.2012.03.044.

(65) Bradley, S. J.; Chi, M.; White, J. M.; Hall, C. R.; Goerigk, L.; Smith, T. A.; Ghiggino, K. P. The Role of Conformational Heterogeneity in the Excited State Dynamics of Linked Diketopyrrolopyrrole Dimers. *Phys. Chem. Chem. Phys.* **2021**, *23* (15), 9357–9364. https://doi.org/10.1039/d1cp00541c.

(66) Lawrance, W. D.; Knight, A. E. W. Unraveling of Vibronically Scrambled Electronic Spectra: The S_2-S_0 Transition in Azulene. *J. Phys. Chem.* **1990**, *94* (4), 1249–1267. https://doi.org/10.1021/j100367a012.

(67) Klemp, D.; Nickel, B. Relative Quantum Yield of the $S_2 \rightarrow S_1$ Fluorescence from Azulene. *Chem. Phys. Lett.* **1986**, *130* (6), 493–497. https://doi.org/10.1016/0009-2614(86)80245-7.

(68) Lewis, J. W. The Spectroscopy of Azulenes., Louisiana State University and Agricultural

& Mechanical College, Ann Arbor, **1979**

(69) Ou, L.; Zhou, Y.; Wu, B.; Zhu, L. The Unusual Physicochemical Properties of Azulene and Azulene-Based Compounds. *Chinese Chem. Lett.* **2019**, *30* (11), 1903–1907. https://doi.org/10.1016/j.cclet.2019.08.015.

(70) Olszowski, A.; Ruziewicz, Z.; Chojnacki, H. Highly Resolved Structure of the Electronic Spectra of Azulene in Frozen Hydrocarbon Matrices. *J. Mol. Struct.* **1975**, *28* (1), 5–24. https://doi.org/10.1016/0022-2860(75)80039-1.

(71) Wagner, B. D.; Tittelbach-Helmrich, D.; Steer, R. P. Radiationless Decay of the S_2 States of Azulene and Related Compounds: Solvent Dependence and the Energy Gap Law. *J. Phys. Chem.* **1992**, *96* (20), 7904–7908. https://doi.org/10.1021/j100199a016.

(72) Gillispie, G. D.; Lim, E. C. Vibrational Analysis of the $S_2 \rightarrow S_1$ Fluorescence of Azulene in a Naphthalene Mixed Crystal at 4.2 K. *J. Chem. Phys.* **1978**, *68* (10), 4578–4586. https://doi.org/10.1063/1.435563.

(73) Andre, J. C.; Viriot, M. L.; Niclause, M.; Ware, W. R. Diffusion Controlled Photosensitization in Liquid Phase. *React. Kinet. Catal. Lett.* **1979**, *12* (1), 39–43. https://doi.org/10.1007/BF02071422.

(74) Awuku, S.; Bradley, S. J.; Ghiggino, K. P.; Steer, R. P.; Stevens, A. L.; White, J. M.; Yeow, C. Photophysics and Spectroscopy of 1,2-Benzazulene. *Chem. Phys. Lett.* **2021**, *784* (October), 139114. https://doi.org/10.1016/j.cplett.2021.139114.

(75) Nunn, J. R.; Rapson, W. S. 178. Cyclic Conjugated Polyenes. Part I. 1 : 2-Benzazulene. *J. Chem. Soc.* **1949**. https://doi.org/10.1039/JR9490000825.

(76) Lou, Y.; Chang, J.; Jorgensen, J.; Lemal, D. M. Octachloroazulene. *J. Am. Chem. Soc.* **2002**, *124* (51), 15302–15307. https://doi.org/10.1021/ja012051h.

(77) Lu, H. M.; Page, J. B. On the Use of Combination/Overtone Band Resonance Raman Excitation Profiles for Understanding the Vibronic Coupling Mechanism in the 700 nm Absorption Band of Azulene. *J. Chem. Phys.* **1990**, *92* (12), 7038–7049. https://doi.org/10.1063/1.458244.

(78) Vosskötter, S.; Konieczny, P.; Marian, C. M.; Weinkauf, R. Towards an Understanding of the Singlet-Triplet Splittings in Conjugated Hydrocarbons: Azulene Investigated by Anion Photoelectron Spectroscopy and Theoretical Calculations. *Phys. Chem. Chem. Phys.* **2015**, *17* (36), 23573–23581. https://doi.org/10.1039/c5cp01826a.

(79) Heritage, J. P.; Penzkofer, A. Relaxation Dynamics of the First Excited Electronic Singlet State of Azulene in Solution. *Chem. Phys. Lett.* **1976**, *44* (1), 76–81. https://doi.org/10.1016/0009-2614(76)80413-7.

(80) Ippen, E. P.; Shank, C. V.; Woerner, R. L. Picosecond Dynamics of Azulene. *Chem. Phys. Lett.* **1977**, *46* (1), 20–23. https://doi.org/10.1016/0009-2614(77)85155-5.

(81) Huppert, D.; Jortner, J.; Rentzepis, P. M. Laser Excited Emission Spectroscopy of Azulene in the Gas Phase. *J. Chem. Phys.* **1972**, *56* (10), 4826–4833. https://doi.org/10.1063/1.1676957.

(82) Tétreault, N.; Muthyala, R. S.; Liu, R. S. H.; Steer, R. P. Control of the Photophysical Properties of Polyatomic Molecules by Substitution and Solvation: The Second Excited Singlet State of Azulene. *J. Phys. Chem. A* **1999**, *103* (15), 2524–2531. https://doi.org/10.1021/jp984407q.

(83) Xin, H.; Hou, B.; Gao, X. Azulene-Based π-Functional Materials: Design, Synthesis, and Applications. *Acc. Chem. Res.* **2021**, *54* (7), 1737–1753. https://doi.org/10.1021/acs.accounts.0c00893.

(84) Xin, H.; Li, J.; Ge, C.; Yang, X.; Xue, T.; Gao, X. 6,6 0 -Diaryl-Substituted Biazulene Diimides for Solution-Processable High-Performance n-Type Organic Semiconductors†. *Mater. Chem. Front.* **2018**, *2* (5), 975–985. https://doi.org/10.1039/c8qm00047f.

(85) Tabachnyk, M.; Karani, A. H.; Broch, K.; Pazos-Outón, L. M.; Xiao, J.; Jellicoe, T. C.; Novák, J.; Harkin, D.; Pearson, A. J.; Rao, A.; Greenham, N. C.; Böhm, M. L.; Friend, R. H. Efficient Singlet Exciton Fission in Pentacene Prepared from a Soluble Precursor. *APL Mater.* **2016**, *4* (11). https://doi.org/10.1063/1.4968518.

(86) Aulin, Y. V.; Felter, K. M.; Günbas, D. D.; Dubey, R. K.; Jager, W. F.; Grozema, F. C. Morphology-Independent Efficient Singlet Exciton Fission in Perylene Diimide Thin Films. *Chempluschem* **2018**, *83* (4), 230–238. https://doi.org/10.1002/cplu.201700449.

A. APPENDICES

ADDITIONAL FIGURES

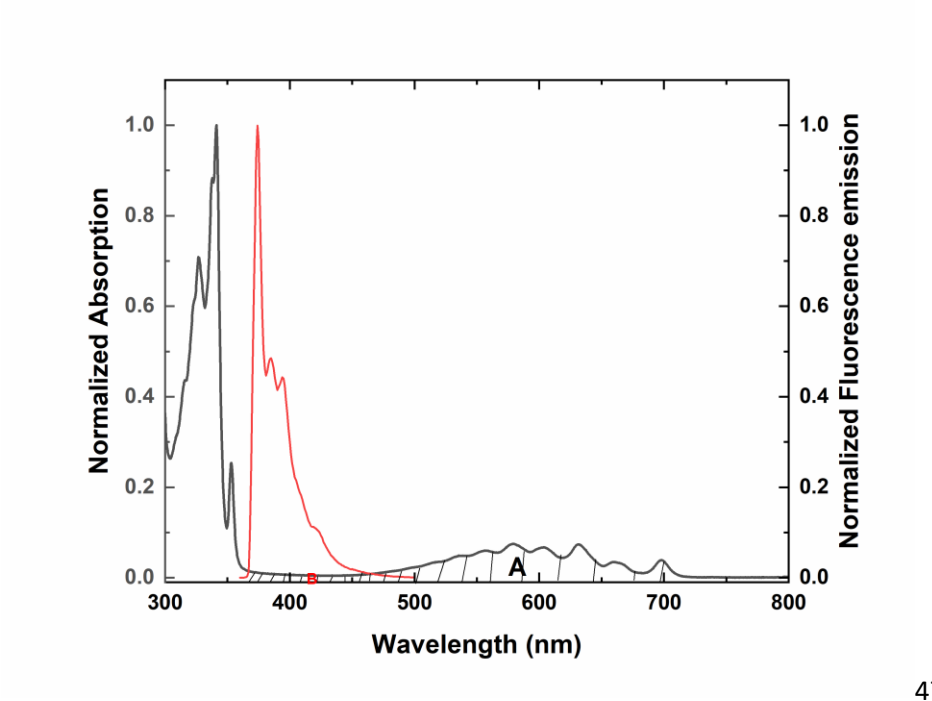

47

Figure A1: Overlap of the $S_2 \rightarrow S_0$ fluorescence and $S_0 \rightarrow S_1$ absorption spectra of azulene. The area of the overlap between these two spectra (B) is estimated to be a factor of 10 times lesser than the whole $S_0 \rightarrow S_1$ absorption spectra (A).

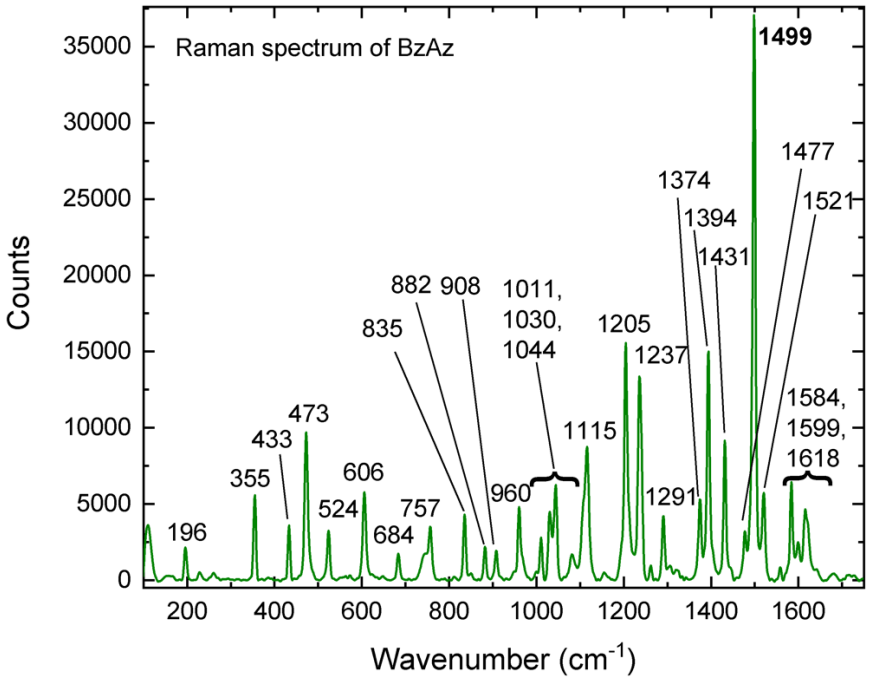

Figure A2A: Raman spectrum of a solid film of 1,2-benzazulene within the range of 100 to 1750 cm^{-1}

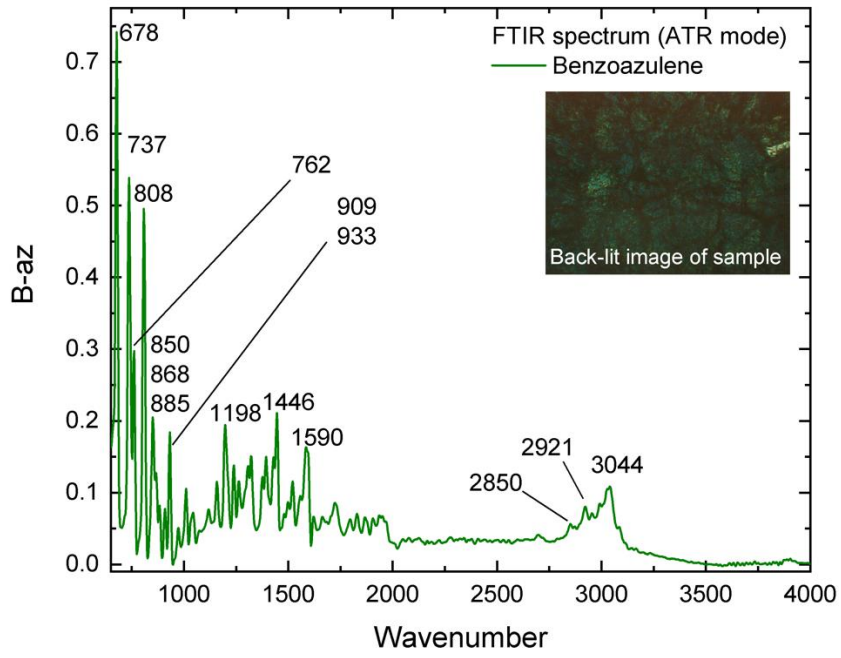

Figure A2B: FTIR spectrum of a solid film of 1,2-benzazulene obtained by the attenuated total reflectance method.

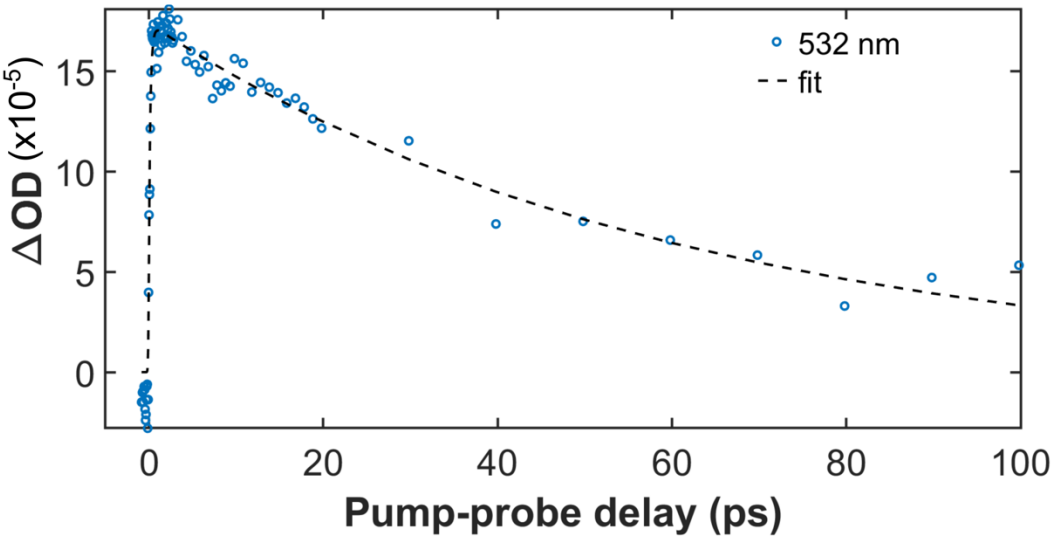

Figure A3: Decay of the transient absorption of 1,2-benzazulene in THF excited at 400 nm and monitored at 532 nm. The decay was fit to a single exponential function of lifetime 65 ps. The average excitation power is 700 μW.

ADDITIONAL CALCULATIONS

Photodegradation Quantum Yield Calculation for 1,2 − benzazulene

1) Calculating the energy of a photon

$$\text{Excitation wavelength} = 355\ \text{nm} = 355 \times 10^{-9}\ \text{m}$$

$$\text{Energy of a photon} = \text{E}$$

$$\text{h} \times \text{f};\ \text{where C} = \text{f} \times \lambda$$

$$\therefore \text{E} = \text{hC}/\lambda\ \text{where}\ (\lambda = 355 \times 10^{-9}\ \text{m})$$

$$= (6.63 \times 10^{-34})\ \text{Js} \times (3 \times 10^{8})\ \text{ms}^{-1} / (355 \times 10^{-9})\ \text{m}$$

$$= (5.603 \times 10^{-19})\ \text{Jphoton}^{-1}$$

2) Calculating the power absorbed by the sample

Amount of power that hits the sample $= P_1 = 5.14 \times 10^{-3}\ Js^{-1}$

Amount of power that transmitted through the sample $= P_2 = 2.80 \times 10^{-3}\ Js^{-1}$

Amount of power absorbed by the sample $= (P_1 - P_2) = \Delta P$

$\Delta P = (5.14 \times 10^{-3} - 2.80 \times 10^{-3})Js^{-1} = 2.34 \times 10^{-3}\ Js^{-1}$

3) Calculating the number of molecules degraded at 403 nm Absorbance (A) wavelength

Absorbance at "0" minutes $= A_1 = 0.324$ OD

Absorbance after "60" minutes $= A_2 = 0.316$ OD

Absorbance difference $= (A_1 - A_2) = \Delta A$

$\Delta A = (0.324 - 0.316)OD = 8 \times 10^{-3}$ OD

Sample concentration $= C = 105.5\ \mu M = 105.5 \times 10^{-6}\ molL^{-1}$

Cuvette volume $= V = 3000\ \mu L = 3 \times 10^{-3}$ L

Number of moles $= C \times V = 105.5 \times 10^{-6} molL^{-1} \times 3 \times 10^{-3}$ L $= 3.165 \times 10^{-7}$ mols

Number of molecules (N) $= C \times V \times L$; (L – Avogadro Number)

$N = 3.165 \times 10^{-7}$ mols $\times 6.02 \times 10^{23} = 1.905 \times 10^{17}$ molecules

Number of molecules decomposed $= \Delta A \times (C \times V \times L)$

Number of molecules decomposed $= 8 \times 10^{-3} \times 1.905 \times 10^{17}$ molecules

Number of molecules decomposed $= 1.524 \times 10^{15}$ molecules

4) Calculating the photodegradation quantum yield (QPD)

$$\text{QPD} = \frac{\text{Number of molecules decomposed per total time}}{\text{Number of photons absorbed}}$$

$$\text{But number of photons absorbed} = \frac{\Delta P}{E} = \frac{2.34 \text{ x } 10^{-3} \text{ Js}^{-1}}{5.603 \times 10 - 19) \text{ Jphoton}^{-1}}$$

$$\text{But number of photons absorbed} = 4.18 \text{ x } 10^{15} \text{ photons}^{-1}$$

$$\text{QPD} = \frac{1.524 \text{ x } 10^{15} \text{ molecules}/3600 \text{ s}}{4.18 \text{ x } 10^{15} \text{ photons}^{-1}} = 1.01 \text{ x } 10^{-4} \text{ molecules photon}^{-1}$$